IEEE Access
Multidisciplinary | Rapid Review | Open Access Journal

Received 19 May 2024, accepted 14 July 2024, date of publication 17 July 2024, date of current version 5 August 2024.

Digital Object Identifier 10.1109/ACCESS.2024.3429633

RESEARCH ARTICLE

TumorGANet: A Transfer Learning and Generative Adversarial Network-Based Data Augmentation Model for Brain Tumor Classification

ANINDYA NAG[1], (Member, IEEE), HIRAK MONDAL[2], MD MEHEDI HASSAN[1], (Member, IEEE), TAHER AL-SHEHARI[3], MOHAMMED KADRIE[3], MUNA AL-RAZGAN[4], TAHA ALFAKIH[5], SUJIT BISWAS[6], (Member, IEEE), AND ANUPAM KUMAR BAIRAGI[1], (Senior Member, IEEE)

[1]Computer Science and Engineering Discipline, Khulna University, Khulna 9208, Bangladesh
[2]Department of Computer Science and Engineering, North Western University, Khulna, Bangladesh
[3]Department of Self-Development Skill, Common First Year Deanship, King Saud University, Riyadh 11362, Saudi Arabia
[4]Department of Software Engineering, College of Computer and Information Sciences, King Saud University, Riyadh 11345, Saudi Arabia
[5]Department of Information Systems, College of Computer and Information Sciences, King Saud University, Riyadh 11543, Saudi Arabia
[6]Department of Computer Science, City, University of London, EC1V 0HB London, U.K.

Corresponding author: Anupam Kumar Bairagi (anupam@cse.ku.ac.bd)

This work was supported by King Saud University, Riyadh, Saudi Arabia, through the Researchers Supporting Project RSP2024R206.

ABSTRACT Diagnosing brain tumors using magnetic resonance imaging (MRI) presents significant challenges due to the complexities of segmentation and the variability in tumor characteristics. To address the limitations inherent in traditional methods, this research employs an advanced deep learning approach, integrating ResNet50 for feature extraction and Generative Adversarial Networks (GANs) for data augmentation. A comprehensive evaluation of ten transfer learning algorithms, including GoogLeNet and VGG-16, was conducted for the classification of brain tumors. Model performance was assessed using precision, recall, and F1-score metrics, complemented by additional metrics such as Hamming loss and the Matthews correlation coefficient to provide a more comprehensive insight. To ensure transparency in image predictions, Explainable AI techniques, specifically Local Interpretable Model-Agnostic Explanations (LIME), were utilized. The study involved the analysis of 7023 MRI images, with TumorGANet being trained on a dataset encompassing gliomas, meningiomas, non-tumorous cases, and pituitary tumors. The results demonstrate the exceptional performance of proposed model named TumorGANet, achieving an accuracy of 99.53%, precision and recall rates of 100%, F1 scores of 99%, and a Hamming loss of 0.2%.

INDEX TERMS Brain imaging, brain tumor, transfer learning, generative adversarial network, explainable AI.

I. INTRODUCTION

Magnetic resonance imaging (MRI) serves as an indispensable tool in comprehending brain anatomy within clinical investigations. This non-invasive technique generates detailed brain images through powerful magnetic fields and radio waves, offering high-resolution insights into brain structure and function. The clarity, contrast, and precise differentiation of soft tissues in MRI scans facilitate accurate disease diagnosis. Precise segmentation of both pathological and healthy tissues within the MRI is crucial for pathology comprehension, studying progression, treatment planning, and identifying optimal surgical approaches [1]. Automated segmentation techniques play a pivotal role by enabling volumetric analysis of pathological MRI signals and offering varying levels of automation to delineate tissue boundaries.

The associate editor coordinating the review of this manuscript and approving it for publication was Mingbo Zhao.

Brain tumors (BT) signify unchecked cell growth, with malignant tumors representing active cancerous cells and benign ones being structurally similar but non-cancerous. Common benign tumors include meningioma and glioma, whereas astrocytomas and glioblastomas are malignant high-grade tumors [2]. Brain and central nervous system (CNS) cancer is a prominent cause of mortality. Based on prior research, it is projected that approximately 18,990 individuals (11,020 males and 7,970 females) will be affected by CNS cancer [3]. In 2020, the global death toll from primary malignant brain and CNS tumors amounted to 251,329 individuals. The American Cancer Society article predicts that there will be approximately 3490 new instances of brain and CNS cancer in 2023. Out of these cases, 1900 are expected to be men, and 1590 are expected to be females. Prompt identification and precise categorization are essential but also highly demanding [4]. The field of neurology is constantly working towards advancements in this area.

Accurate segmentation of both pathological and healthy brain tissues from MRI scans, along with their associated sub-regions, is essential for devising effective cancer treatment strategies and advancing cancer research [5]. A BT MRI provides crucial details to physicians, including the tumor's location, size, shape, irregularities, and intra-tumoral structure, aiding qualitative or quantitative analysis. This information assists in determining the tumor's growth stage and evaluating the effectiveness of treatments [6]. However, it's important to note that substantial volumes of data are necessary to train machine learning (ML) or deep learning (DL) models for medical image analysis. Image segmentation, which involves isolating regions of interest, remains a pivotal yet time-consuming task in various medical image processing techniques due to the abundance of data in each image. Radiologists typically consider multiple MRI techniques simultaneously for BT image segmentation [7]. Traditional survival prediction methods heavily rely on the manual extraction of a few characteristics from MRI data, which is labor-intensive, time-consuming, and subjective, posing a challenge for automated analysis [8].

A. MOTIVATION

Image processing and transfer learning (TL) approaches are commonly employed in BT detection research to enhance the accuracy of the model. The primary obstacles in this domain encompass the diverse array of tumor classifications, the spatial arrangement of the tumors, and the skewed or restricted dataset. Tumors can vary in size and location inside the brain. This poses a challenge for the model in accurately categorizing tumor types. Several datasets in this domain exhibit constraints or disparities, leading to biased learning outcomes. These issues are apparent in our work. Several investigations [9], [10], [11], [12] documented a lack of precision in their models. The datasets [13], [14], [15] utilized in certain research studies were either restricted in size or exhibited substantial disparities in class distribution. This has the potential to impact the model's performance. Some instances faced difficulties in achieving satisfactory accuracy, even while employing a less complex three-group model [16]. Strategies for tackling challenges like differences in tumor sizes and locations are not addressed by Khairandish et al., [17]. Moreover, the specific features utilized by their models to produce predictions are not discernible. Nevertheless, S.Babu et al., [18] conducted applied the layer-wise relevance propagation (LRP) technique and included heatmaps to enhance the interpretability of the model. Although employing this approach, their precision is inferior in comparison to our model. In addition, they omitted the pre-processing of the data and instead prioritized a more targeted training approach based on specific classes.

Tackling these problems could result in the development of more resilient and precise MRI BT detection systems. The objective of our research is to address these deficiencies. The objective is to enhance the detection of BT in MRI scans by constructing a model that takes into account tumor sizes, locations, and unbalanced datasets, while simultaneously preserving model transparency.

B. CONTRIBUTION OF THIS STUDY

A novel strategy has been embraced to segment and classify brain tumors (BT), aiming to develop an MRI-based tumor classification model. The objective is to employ a variety of methods to classify BT using deep learning (DL) models. Transfer learning (TL) stands out as an advantageous approach compared to Convolutional Neural Networks (CNNs) alone due to its ability to leverage learned features from one task and apply them to another. The overall contributions of our study are given below.

- Developed a DL approach for BT classification using MRI, leveraging ten pre-trained TL CNN networks, including GoogleNet, DenseNet-121, and VGG-16.
- Utilized ResNet-50 for feature extraction and GANs for data augmentation to enhance model capability and performance.
- Implemented GANs-based augmentation to diversify MRI datasets, mitigate imbalances, and improve model generalization and classification accuracy.
- Conducted a four-class classification and assessed results using standard benchmark measures, with the proposed framework outperforming existing models.
- Employed Explainable AI using LIME to ensure transparency and accountability, highlighting focused features or locations in image predictions.
- Introduced a novel approach by combining VGG-16 with GANs-based data augmentation, enhancing feature representation and providing comprehensive insights for accurate BT diagnosis.

The subsequent sections of the paper are partitioned and structured in the following manner: Section II covers a literature review, Section III describes the Dataset, Section IV outlines the Model Architecture, Section V

presents the proposed Method, and Section VI showcases the experimental results and a comparison with other recent state-of-the-art methods. Section VII provides an Ablation Study. Section VIII provides features to explain ability analysis. Experimentation with prior research is presented in Section IX, and Section X provides the discussion about our proposed model. Section XI has the conclusion of this research and suggestions for future research.

II. RELATED WORKS

A. ML-BASED APPROACHES TO IDENTIFY BT

Chen et al. [13] created an image-processing system based on support vector machines (SVM) to recognize BT. Woldeyohannes et al. [14] also created a classifier model using SVM that used a combination of feature extraction and reduction techniques to classify MRI images as either normal or tumorous. Upgraded K-means clustering techniques were employed during the segmentation phase, specifically on BT images. Saeed et al. [15] developed a system that utilizes 4D image light field techniques to differentiate cancer-affected regions from non-tumor areas. Their methodology included a hybrid K-Nearest Neighbor (k-NN) technique in conjunction with Laplace transform, Fast Fourier transform, and four-dimensional MRI scans.The utilization of ML for BT classification from MRI encounters difficulties such as restrictions in interpretability and the requirement for diverse, high-quality labeled data to address overfitting and assure generalizability.

B. DL-BASED APPROACHES TO IDENTIFY BT

Utilizing DL to prioritize the reduction of time complexity in this field. Rahman et al. [16] introduced a DL-based method for BT categorization. To mitigate overfitting, the researchers used dropout regularizer and batch normalization techniques. Additionally, they proposed a parallel deep CNN (PDCNN) architecture, which enables the simultaneous extraction of both local and global information. Khairandish et al. [17] introduced a methodology employing a hybrid CNN and SVM algorithm for distinguishing between benign and malignant BT in images. However, the study's limitation lies in its neglect of precise tumor localization within the brain. Therefore, there is a need for further enhancements to address this limitation. Babu et al. [18] introduced an abnormal-to-normal translation generative adversarial network. Their approach aimed to convert medical images containing lesions into corresponding images where the lesions are ''removed.'' Asif et al. [19] developed a CNN-based DL method for identifying BT from MRI scans. Enhancing the system's performance can be achieved through the utilization of larger datasets and the exploration of additional deep-learning techniques. Wang et al. [20] introduced a novel cross-level connected U-shaped networking model (CLCU-Net) designed for precise segmentation of BT from MRI data. Nevertheless, the model exhibits several limitations. Notably, the experiments were conducted utilizing two-dimensional images instead of three-dimensional MRIs, disregarding the inter-slice relationships in the data. A new 3D FCN approach was showcased for tumor cell segmentation in MRI images. However, additional investigation is needed to assess the efficacy of different normalization functions, such as batch normalization with variable batch sizes, layer and group normalization, and instance and local response normalization [21]. Shehab et al. [22] proposed an automated technique for segmenting brain images to address the gradient problem in DNNs. The methodologies presented showed significant improvements in accuracy compared to DNNs, potentially expediting the training process. Rehman et al. [23]introduced the BrainSeg-Net model, employing an encoder-decoder architecture featuring a feature enhancer (FE) block for effective feature extraction. Human segmentation processes are often laborious and error-prone. Al-Saffar et al. [24] devised an automated approach to identify and classify different phases of brain gliomas. Deshpande et al. [25] employed a super-resolution technique that amalgamates CNN methods to enhance accuracy in classifying BT. Various image segmentation algorithms were briefly outlined by Pooja et al. [26]. DL for MRI-based BT classification demands a lot of computer power and data, rendering it unsuitable for real-time clinical use.

C. TL-BASED APPROACHES TO IDENTIFY BT

TL uses pre-trained models to classify BT using MRI faster than typical ML and DL methods by reducing the need for labeled data and processing resources. Shah et al. [27] devised a robust EfficientNet-B0 model aimed at identifying BT in MRI images. Although their research concentrated on exploring five different convolutional models and TL methods, further investigation is warranted. Mahmud et al. [28] conducted a comparison between a CNN architecture and ResNet-50, VGG16, and Inception-v3 models. They found that the CNN architecture outperformed the other models. Srikanth et al. [29] created a 16-layer VGG-16 deep neural network to classify BT MR images into many categories. Process automation streamlines diagnosis operations with Samee et al., [30]'s GN-AlexNet model for BT tri-classification. When testing on imbalanced datasets, model performance may be biased and minority class predictions inaccurate. Gupta et al.'s [31] Modified InceptionResNetV2 pre-trained framework for BT detection and radiomics feature-based tumor (RFT) classification is simpler and faster, improving computing efficiency and diagnosis time. However, model accuracy and generalization may be limited compared to more complicated systems. Alqazzaz et al. [32] utilized a SegNet model tailored for MRI modalities within three-dimensional datasets, enabling autonomous segmentation of BT and their sub-tumor components. However, a notable drawback is the extensive time requirement during the training phase, which can be considered a limitation. Table 1 provides an overview of the diverse methods utilized for classifying BT.

TABLE 1. Summary of the several approaches used to categorize BT.

Reference	Approaches	Model Used	Dataset Used	Accuracy (%)	Explainability
Oksuz et al., (2022) [33]	ML	SVM and KNN classifiers	Figshare BT dataset - 2017	97.25	No
Tahia et al., (2021) [34]		CNN	Kaggle BT MRI Dataset-2021	92	No
Hashemzehi et al., (2020) [35]		CNN-NADE	Kaggle BT Classification (MRI)-2021	95	No
Lamrani et al., (2022) [36]		CNN	Kaggle BT MRI Dataset-2021	96	No
Kadry et al., (2019) [37]	DL	Hybrid DL-based Model	ISLES-2015 and BRATS-2015	96	No
Ismael et al., (2019) [38]		Residual networks	Figshare BT dataset-2017	97	No
Nayak et al., (2022) [39]		Deep autoencoder approach	Kaggle BT MRI Dataset-2021	97	No
Kokkalla et al., (2021) [40]		Deep inception residual network	Kaggle BT MRI Dataset-2021	97.69	No
Kesav et al., (2022) [41]		RCNN-based model	Kaggle BT MRI Dataset-2021	98.21	No
Ali et al., (2022) [42]		CNN with VGG-19 encoder	BRATS-2020	83.01	No
Hong et al., (2022) [43]		3D FRN-ResNet	Clinical MDD sMRI images dataset	86.78	No
Krishnasamy, N. et al., (2023) [44]		FCNs + ResNet	Kaggle BT MRI Dataset-2021	93.90	No
Zhaid U. et al., (2022) [45]		ResNet-101	BraTS-2018	94.40	No
Ullah N et al., (2022) [46]		Inceptionresnetv2	Kaggle BT Classification (MRI)-2020	98.91	No
Tummala et al., (2022) [47]		ImageNet-based ViT	Figshare Brain MRI Dataset-2021	98.70	No
Cinar et al., (2022) [48]	TL	UNet + DenseNet-121	BRATS-2019	95	No
Gaikwad, S. et al., (2023) [49]		EfficientNetV2B1	Kaggle BT MRI Dataset-2021	97.4	No
Srikanth et al., (2021) [29]		16-layers VGG-16 deep NN	OECD Statistical Yearbook dataset	98	No
Ullah N et al., (2024) [50]		DeepEBTDNet	Kaggle BT Detection MRI-2021	98.96	Yes
Haque, R., et al., (2024) [51]		NeuroNet19	Kaggle BT MRI Dataset-2021	99.30	Yes
Ullah N et al., (2022) [52]		TumorResNet	Kaggle BT Detection (Br35H)-2020	99.33	No
Raza et al., (2022) [53]		DeepTumorNet	Kaggle BT Detection (Br35H)-2020	99.33	No

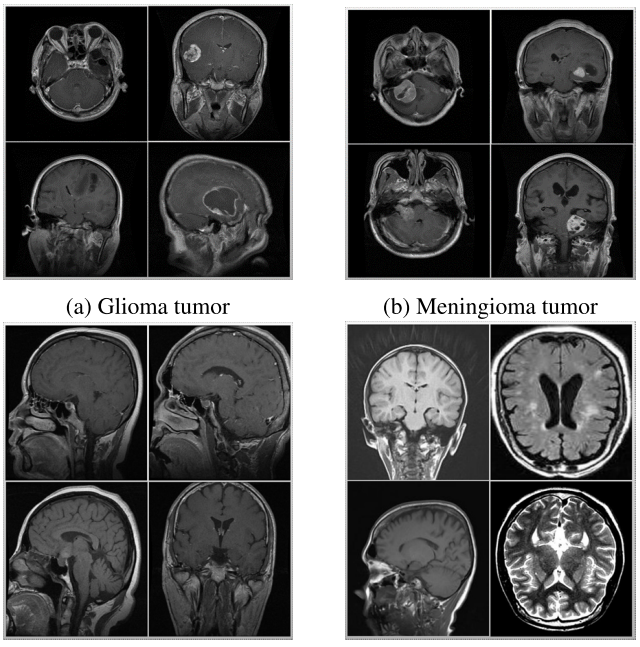

(a) Glioma tumor (b) Meningioma tumor

(c) Pituitary tumor (d) No tumor

FIGURE 1. Sample images from each class.

III. DATASET

This study utilized the BT MRI dataset. The Kaggle website now includes the first publicly available collection of brain MRI images. This dataset comprises 7023 MRI images, of which 1311 images go under the testing category and 5712 images come under the training category. The four classes in this dataset are glioma, meningioma, pituitary, and no tumor. Before being delivered to the model, these MRI images undergo pre-processing. The dataset consists of training and testing samples for various types of cancers. The numerous tumor types, such as glioma tumor, meningioma tumor, no tumor, and pituitary tumor, are given in the ''Name of Tumor'' column. The ''Training'' column indicates the number of training samples that are available for each type of tumor, with 1321 samples for gliomas, 1339 samples for meningiomas, 1595 samples for no tumor, and 1457 samples for pituitary tumors. Similar to that, ''Testing'' indicates the number of testing samples for each type of tumor, with 300 samples for gliomas, 306 for meningiomas, 405 for no tumors, and 300 for pituitary tumors. Images from each class are shown in Figure 1. Table 2 provides Number of the MRI pictures of the training and testing datasets for glioma, meningioma, pituitary, and no tumor.

TABLE 2. Number of MRI images in training and testing datasets.

Name of Tumor	Training	Testing	Total
Glioma tumor	1321	300	1621
Meningioma tumor	1339	306	1645
Pituitary tumor	1457	300	1757
No tumor	1595	405	2000
Total	5712	1311	7023

IV. PROPOSED MODEL ARCHITECTURE (TumorGANet)

Figure 2 illustrates the data flow diagram of the proposed TumorGANet model. We employ ResNet-50 as a means of extracting features. Subsequently, we utilize GANs for data augmentation. Finally, we apply 10 distinct transfer learning algorithms to classify BT. Figure 3 presents the architecture of the proposed model, including detailed information about each part.

A. PSEUDO-CODE FOR PROPOSED MODEL (TumoGANet)

Below is the pseudo-code for the whole TumorGANet architecture.

V. METHODS

Figure 5 illustrates the working procedure of the provided methodology. The technique comprises four primary stages: Data preprocessing, Feature extraction using the ResNet-50 model, Data augmentation using GANs, and implementation of the applied transfer learning algorithms. The specificities

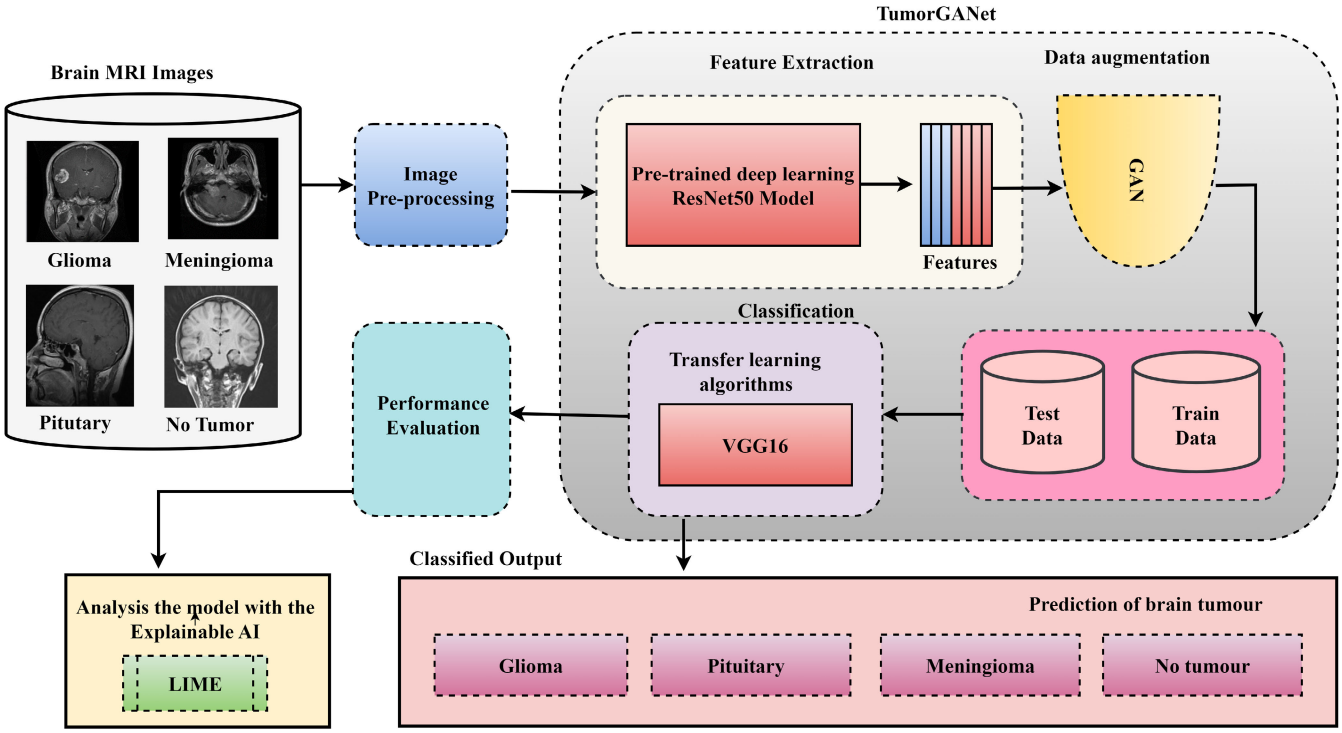

FIGURE 2. Data flow diagram of proposed TumorGANet model.

of each of these phases are outlined in the following subsections.

A. DATA PREPROCESSING

Let's examine a set of BT MRI images Z, consisting of j images.

$$Z = \{Z_1, Z_2, \ldots, Z_i, \ldots, Z_j\}, \tag{1}$$

The variable Z_i represents the i^{th} input image, whereas j represents the total number of images. Preprocessing makes raw data understandable. It also reduces distortions and improves image attributes, speeding up processing. The pre-processing stage receives the brain picture Z_i, and its appraisal is crucial. Pre-processing ensures uniformity. Additionally, the image exhibits irregular lighting. Uneven lighting may be caused by filament deterioration or sick apertures. MRI intensity levels often change. The acquisition circumstance greatly affects MRI scan intensity. The acquisition scenario affects MRI intensity. Normalization ensures comparability. Adjusting image size improves efficiency and reduces memory usage. Below are some preprocessing methods we used in this work. There were several stages to preprocessing brain MRI pictures. The operations include scaling, shearing, zooming, and horizontal flipping. Figure 4, shows a preprocessed image by applying preprocessing techniques to each image.

1) IMAGE RESIZING

Resizing images is essential for several purposes, including maintaining constant input sizes, improving computational efficiency, reducing overfitting, augmenting the dataset, addressing memory limitations, facilitating transfer learning, and enhancing inference speed. Resizing images appropriately enhances the ability of neural networks to acquire significant features and patterns. The images have been resized from 512×512 pixels to 224×224 pixels.

Let, $(W_{original}, H_{original})$ represent the dimensions of the original image, and (W_{new}, H_{new}) represent the dimensions of the new image.

The scaling factor for width (SF_w) and height (SF_h) can be determined using the following formula:

$$SF_w = \frac{W_{new}}{W_{original}}, \quad SF_h = \frac{H_{new}}{H_{original}} \tag{2}$$

The new coordinates (x_{new}, y_{new}) for a point (x, y) in the original image can be derived using the following formula:

$$x_{new} = x \times SF_w, \quad y_{new} = y \times SF_h \tag{3}$$

2) IMAGE SCALING

It transforms the outcome of mathematical calculations into a visually representable form and is frequently employed to modify picture attributes such as brightness, contrast, and other features in jobs related to image processing and computer vision. We have employed a value of 1.00 for parameter a to regulate brightness and a value of 0 for parameter b to control contrast. Image pixels are scaled down here. Original 8-bit color graphics have pixel values from 0 to 255. Divide all pixel values by 255 to get a 0-1 range. Normalizing pixel values for training speeds neural network convergence and maintains gradient consistency.

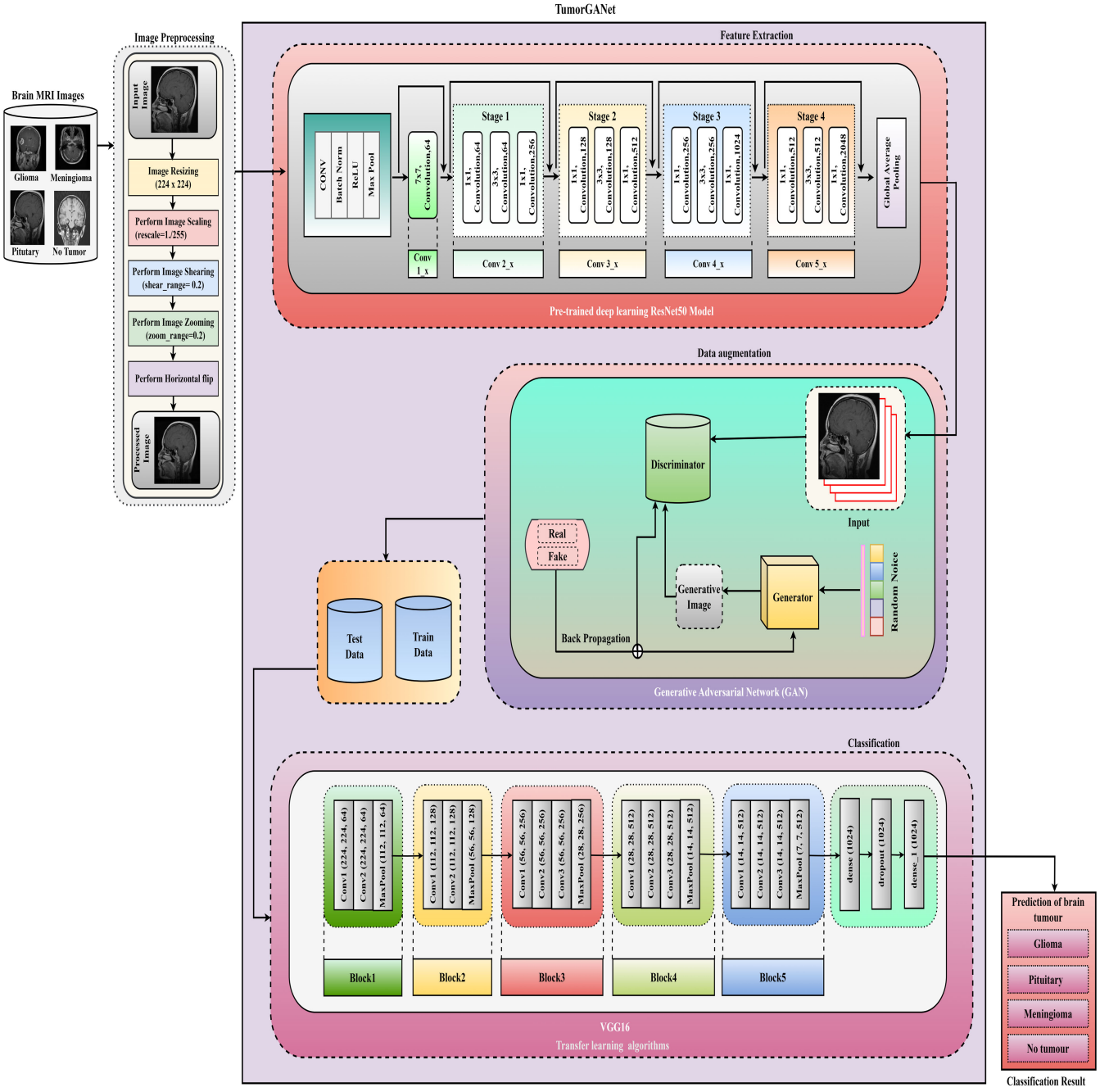

FIGURE 3. Stepwise proposed methodology of this paper.

The mathematical equation for picture scaling, specifically for standardizing pixel values in the context of image processing, can be stated as follows:

$$NormalizedPixelValue = \frac{OriginalPixelValue}{255} \quad (4)$$

The *OriginalPixelValue* refers to the numerical value assigned to a pixel in an image before the process of normalization. The maximum pixel value for an 8-bit color graphic is *255*. The *Normalizedpixelvalue* refers to the pixel value that has been scaled to fit within the range of *0 to 1*.

To modify the brightness, the converted pixel value can be determined using the formula, where parameter a controls the brightness and parameter b controls the contrast.

$$TransformedPixelValue = a \times OriginalPixelValue + b \quad (5)$$

The value of a is set to *1.00* for adjusting the brightness, while the value of b is set to *0* for controlling the contrast. This scaling approach ensures pixel values are within a standard range. This helps neural networks converge during training and maintain gradient constancy.

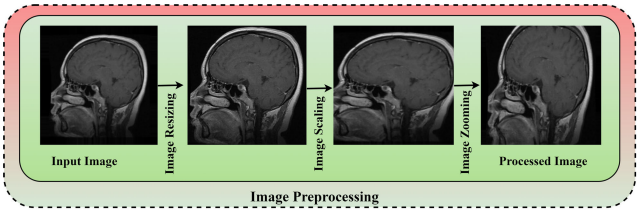

FIGURE 4. Step-wise reprocessing steps are shown for preparing final training images of our proposed model.

3) IMAGE ZOOMING

Following the scaling operation, we zoomed the image to enhance its visual quality. Image zoom transformation randomly zooms in or out. The zoom range option controls zooming. Images can be zoomed 20% with a zoom range of 0.2. Training on diverse dimensions and perspectives of the same items strengthens the model.

The zoom transformation, which randomly zooms in or out of an image, has the following mathematical formula:

$$\begin{aligned} &ZoomedPixelValue \\ &= OriginalPixelValue \\ &\quad \times (1 + ZoomRange \times (RandomValue - 0.5)), \end{aligned} \tag{6}$$

The *OriginalPixelValue* refers to the value of a pixel in an image before any zooming or magnification. The *ZoomRange* refers to the designated range for random zooming, such as *0.2* for a 20% *ZoomRange*. The *RandomValue* is a stochastic variable that is uniformly distributed between *0 and 1*. This formula utilizing a random zoom factor resales pixel values to zoom in (values greater than 1) and out (values less than 1). Randomness during training improves the model's ability to handle diverse dimensions and viewpoints of the same concept, increasing diversity.

We then use a horizontal flip. This option turns photos horizontally randomly when set to true. It means certain photos will be horizontally mirrored during training, which might boost dataset diversity. In tasks where object orientation doesn't matter, this augmentation is common. A horizontal flip transformation randomly mirrors an image using the following formula:

$$\begin{aligned} &FlippedPixelValue(i, j) \\ &= OriginalPixelValue(i, Width - 1 - j), \end{aligned} \tag{7}$$

Here, $OriginalPixelValue(i, j)$ represents the pixel value at (i, j) in the original image. The $FlippedPixelValue(i, j)$ represents the pixel value at $(i, \text{Width} - 1 - j)$ after horizontal flipping. To flip the image horizontally, this formula reverses pixel values along the width axis. Randomly creating horizontally mirrored images during training can enhance dataset diversity for tasks where object orientation is not crucial. Figure 4 depicted the image after undergoing a series of sequential processing processes.

B. DATA AUGMENTATION USING GANs

After preposing, we extract features using pre-trained ResNet-50 deep learning. We augmented the data with GANs. Next, we partition the data into training and test sets. These data augmentation methods boost training data diversity to improve neural network performance and decrease overfitting. Randomly applying these modifications to training photos helps the model become more resilient and generalize to new data. GANs may be employed for data augmentation by training the generator architecture to generate novel pictures based on the input data [54]. The produced images may be incorporated into the training set, thereby enlarging the dataset and providing additional examples for the model to acquire knowledge from. Expanding

Algorithm 1 Pseudo-Code of TumorGANet

Start
Input: MRI brain images. Labels, Performance Metrics, Best Model Insights.
Step 1: Read the original MRI brain images.
Step 2: Perform Image Processing.
- Perform Image Resizing
- Perform Image Scaling
- Perform Image Shearing
- Perform Image Zooming

Step 3: Feature Extraction using ResNet-50.
Step 4: Data Augmentation using GANs.
- Initialization:
  - Initialize generator, discriminator, and GANs with suitable architectures.
  - Compile discriminator and GANs with appropriate settings.
- Training Loop:
  - For each epoch in range (epochs):
    - ◇ Train Discriminator:
      - ▷ Sample *half_batch* real images and generate *half_batch* fake images.
      - ▷ Update discriminator parameters using binary cross-entropy loss.
      - ▷ Calculate *d_loss* as the average of losses for real and fake images.
    - ◇ Train Generator:
      - ▷ Generate *batch_size* random noise samples.
      - ▷ Update generator parameters using binary cross-entropy loss with discriminator output.
      - ▷ Calculate *g_loss* as the binary cross-entropy loss between generated images and labels.
- After Training:
  - Generate *X_augmented* by feeding random noise through the trained generator.

Step 5: Split Dataset into Training and Test Sets.
Step 6: Apply Transfer Learning Algorithm.
Step 7: Prediction of BT.
Step 8: Evaluate Performance.
Step 9: Analyze the Best Model with Explainable AI.
Output: Predicted Tumor
End

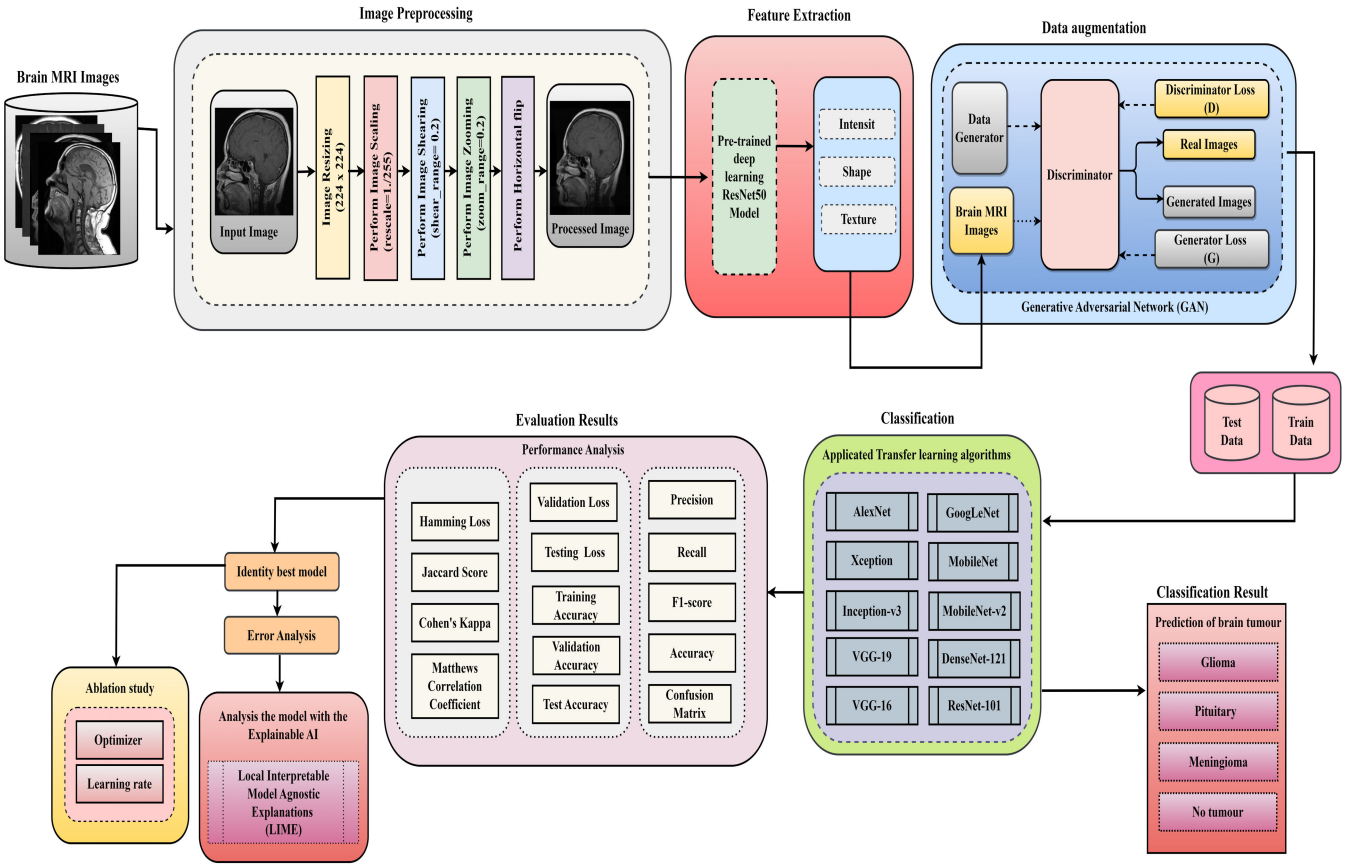

FIGURE 5. The overall workflow of this study.

the dataset can improve the model's performance and reduce overfitting by offering a wider range of training instances. Another approach to using GANs for data augmentation involves utilizing the generator network to generate pictures resembling the test data, which can subsequently be used to expand the test set. Implementing this approach can enhance the model's resilience and fortify it against fluctuations in the test data. Additionally, there is a possibility to optimize the generator network on a specific dataset, enabling the creation of novel images that display comparable attributes [55]. This strategy is advantageous, particularly when dealing with datasets that have restricted data availability. Furthermore, it is crucial to examine the quality of the produced pictures and test the model's performance on a larger dataset to confirm the effectiveness of the data augmentation approach. A fundamental GANs is mathematically formulated with two primary components: the generator (G) and the discriminator (D). The goal is to instruct the generator to produce authentic samples and the discriminator to differentiate between actual and created samples. The objective function of the GANs is expressed as:

$$rClmin_G max_D V(D, G) = \mathbb{E}_{x\sim p_{\text{data}}(x)}[\log D(x)] + \mathbb{E}_{z\sim p_z(z)}[\log(1 - D(G(z)))], \quad (8)$$

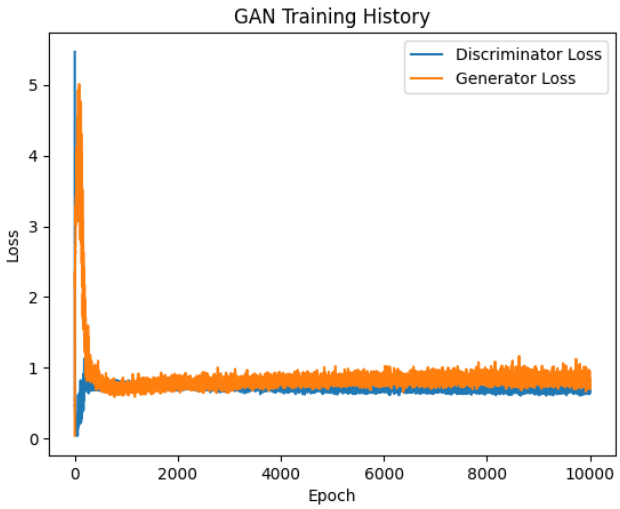

FIGURE 6. GANs training history.

The generator G network receives random noise as input and produces synthetic samples denoted as $G(z)$. The discriminator D network receives samples x and $G(z)$ as input and produces the probability that a sample is genuine. $\mathbb{E}_{x\sim p_{data}(x)}[\log D(x)]$ anticipated outcome of observing actual data samples. The discriminator's objective is to optimize this

parameter, ensuring that $D(x)$ approaches a value of 1 for genuine samples x. $\mathbb{E}_{z\sim p_z(z)}[\log(1 - D(G(z)))]$ anticipated outcome of the generated samples. The objective of the generator is to optimize this parameter, resulting in $D(G(z))$ approaching a value near 0 for the generated samples $G(z)$.

Figure 6, displays the relationship between the number of training epochs and the loss curve of GANs. This research uses brain MRI scans to train GANs to create brain MRI images. We compare GANs model losses between real-world and created images for BT positive and negative cases. We use kernel density estimation (KDE) to compare the density curves of the actual and generated photos and show the results. The density curves of actual and synthesized photos are graphed for BT present and absent. The density curve of images with BT reveals a peak at the tumor location, indicating a higher pixel concentration there. However, the density curve of the generated photographs includes a peak, suggesting they may be less accurate than the originals. The image density curves show a rather homogeneous pixel density distribution without the BT. However, the density curve of the generated images has a comparable distribution with a small peak around the brain's center, suggesting they are more precise and lifelike. The intricate tumor composition and absence of positive examples in the dataset may explain the difference in density distributions of genuine and generated BT images. The image may not accurately depict the tumor's details, causing a density curve peak.

GANs is utilized in this study to address the challenges of data imbalance and limited availability of diverse MRI images for brain tumor classification. GANs generate realistic synthetic samples that enhance the diversity of the training dataset, mitigating imbalances and improving model generalization. This augmentation technique allows the model to learn more robust features, adapt to different clinical scenarios, and reduce overfitting. By incorporating GANs, we enhance the model's capability to accurately classify brain tumors, thereby optimizing data efficiency and classification accuracy.

C. APPLY TRANSFER-LEARNING

TL is a technique in machine learning that leverages knowledge gained from a pre-trained model on one task to enhance performance on a related task. Two prevalent approaches in machine learning include fine-tuning, which entails modifying a pre-trained model to suit a particular task, and feature extraction, which utilizes previously obtained characteristics to train a new classifier. Domain adaptation is to minimize disparities in distributions between the source and target domains, while model pre-training entails initializing a fresh model with weights acquired from a pre-existing trained model. Multi-task learning refers to the training of a model to simultaneously handle multiple tasks. These solutions are essential in situations where there is a limited availability of labeled data for the desired job. They provide a pragmatic approach to enhance model efficiency and accelerate training in specific domains. We employ various transfer learning algorithms for feature extraction and modeling.

1) FEATURE EXTRACTION

Using the ResNet-50 model as a feature extractor for an MRI image dataset entails adapting the pre-trained model to capture significant visual representations. The ResNet-50 model has been loaded, and its top classification layer has been removed, preserving the model's convolutional basis. The images undergo preprocessing to adhere to the input specifications of ResNet50. Afterward, the preprocessed images are subjected to the modified ResNet-50, which applies feature extraction on deeper layers that contain hierarchical representations of visual content. The embeddings, also known as features, offer a comprehensive and conceptual depiction of the pictures. The process of extracting features may be highly beneficial when using pre-trained deep learning models for transfer learning or for providing inputs for downstream tasks such as grouping, similarity comparison, or visualization. Thorough deliberation should be given to the layer from which features are taken, as it impacts the amount of abstraction that is recorded. The resulting embeddings can serve as a foundation for additional study, offering a succinct depiction of the visual characteristics of the MRI data that were acquired by the ResNet-50 model.

2) MODEL BUILDING

We utilized GoogLeNet, DenseNet-121, MobileNet, VGG-19, MobileNet-v2, AlexNet, Xception, ResNet-101, Inception-v3, and VGG-16 for constructing the models. GoogLeNet is an advanced CNN architecture primarily designed for image classification. The main innovation in GoogleNet is the integration of the Inception module, which employs several convolutional filters of different sizes (1×1, 3×3, and 5×5) to capture input at many scales simultaneously. DenseNet-121 is a CNN architecture that is renowned for its dense connectivity and effective parameter sharing. This architecture, belonging to the DenseNet family, features a distinct design in which every layer is intricately related to all other layers [48]. MobileNet is a neural network structure specifically engineered to optimize performance on devices that have restricted resources, such as mobile phones and edge devices [43]. The method addresses the challenges presented by limited computer resources by employing depth-wise separable convolutions. MobileNet-v2 is a tailored iteration of MobileNet that is specifically optimized for use on mobile and edge devices. It utilizes innovative design ideas to overcome constraints in the resources that are already accessible. The model employs inverted residuals to improve feature representation by extending and projecting block information. VGG-19 is a CNN design that is renowned for its straightforwardness and efficiency in applications related to image categorization. The model's architecture is an expansion of the VGG16 model, with a total of 19 layers [42]. AlexNet, an innovative CNN, played a pivotal part in the resurgence of deep learning.

AlexNet's architecture consists of five convolutional layers, followed by three fully connected layers [12]. Xception is a sophisticated CNN architecture that deviates from traditional convolutional designs. This approach is remarkable because it utilizes depth-wise separable convolutions, which effectively isolate the spatial and cross-channel correlations. ResNet-101 is a CNN design that use residual learning to efficiently train networks with a significant number of layers. The ResNet-101 architecture is an expansion of ResNet, with 101 levels [45]. Residual blocks, which incorporate shortcut connections, allow the network to acquire residual functions instead of only transforming inputs into outputs. Inception-v3 is a sophisticated CNN that improves and broadens the capabilities of the original Inception model [44]. The primary objective of this ResNet-101 is to precisely categorize images and identify objects. The main progress is in the use of inception modules, which combine many kernel sizes (1×1, 3×3, 5×5) to efficiently capture characteristics at various scales. The VGG-16 architecture is a CNN that consists of 16 layers and is highly skilled in performing image classification tasks [56]. The design employs a sequence of 3×3 convolutional layers, guaranteeing a consistent receptive field for capturing intricate features.

D. MODEL PARAMETERS TUNING

Model tuning refers to the empirical procedure of identifying the most favorable settings for hyperparameters to optimize model performance. We employ various hyperparameters to fine-tune our suggested model.

1) EPOCH

An epoch (E) signifies a single iteration over the full training dataset. During training, the model parameters are updated E times. The update rules are contingent upon the optimizer, batch size, and learning rate. For each E, the model estimates loss, analyses dataset occurrences, and optimizes parameters.

2) OPTIMIZER

Optimizer assigns optimal ML model training parameters. This strategy minimizes the error or loss function, which compares expected and actual values. Popular optimizers include stochastic gradient descent (SGD), Adam, RMSprop, and Adagrad. SGD adjusts model parameters in the steepest loss function fall. Adjust Adam's RMSprop and Momentum learning rates. RMSprop modifies parameter learning. Adagrad adjusts learning rates using gradients. Optimizers affect neural network training convergence and stability. Denote the weight matrix as W, the learning rate as α, and the gradient of the loss function as ∇L. The weight update equation for SGD can be expressed as follows:

$$W_{new} = W_{old} - \alpha \cdot \nabla L, \tag{9}$$

The Adam optimizer updating rule can be represented by a single mathematical equation as follows:

$$\theta_{t+1} = \theta_t - \frac{\alpha}{\sqrt{\hat{v}} + \epsilon} \cdot \hat{m}_t, \tag{10}$$

where θ_t represents the parameter vector at the current time step t. The parameter vector θ_{t+1} represents the updated values at the next time step $(t+1)$. $\hat{m}_t$ refers to the bias-corrected first-moment estimate. $\hat{v}_t$ refers to the bias-corrected estimate of the second moment. ϵ is a minute constant that is included to ensure numerical stability.

3) LEARNING RATE

ML Learning Rate (α) controls optimization increments and model learning speed. α, that exceeds ideal parameters might cause training divergence or oscillation. The low value of α can hinder convergence and produce unsatisfactory solutions. In training, α schedules and adaptive algorithms like Adam and RMSprop dynamically change α [53].

4) DROPOUT RATE

The dropout rate influences how many neurons are ''dropped out'' during neural network training. This regularisation reduces randomness overfitting. Dropout rate-specified neurons are randomly assigned zero each epoch. Dropout impacts hidden neural network layers, not input or output. During training, the output is produced as the element-wise product of the input input input and a binary mask with values selected from a Bernoulli distribution with dropout rate p.

$$Output = Input \odot mask, \tag{11}$$

where $\odot$ denotes element-wise multiplication.

5) TOTAL BATCH SIZE

Total batch size (B) is the number of examples per model training iteration. The mini-B collects data points processed per iteration. Memory and processing efficiency depend on B. The memory may be needed to increase the B for hardware efficiency. Smaller B allow frequent model parameter changes but slower calculation. The size of the dataset, model complexity, and processing resources determine B.

6) ACTIVATION FUNCTION

Neuron output is mathematically processed by activation functions in neural network layers. Non-linearity helps networks learn complicated patterns. The Rectified Linear Unit (ReLU), Sigmoid, and hyperbolic-tangent activation functions are common activation functions. The sigmoid function compresses input values to 0-1, making it helpful for binary classification. Artificial neural network hidden layers compress input values from -1 to 1 using the hyperbolic tangent function. Neural networks model complex processes and learn and generalize using non-linear activation functions. ReLU, which zeros negative input values but leaves positive input values unchanged. Activation functions assist the model in understanding complex data interactions in forward and backward passes during training. ReLU activation function is formally defined as:

$$ReLU(x) = max(0, x), \tag{12}$$

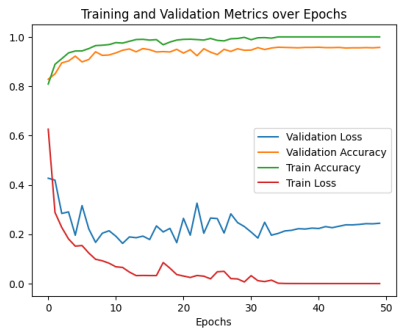

(a) GANs + GoogLeNet

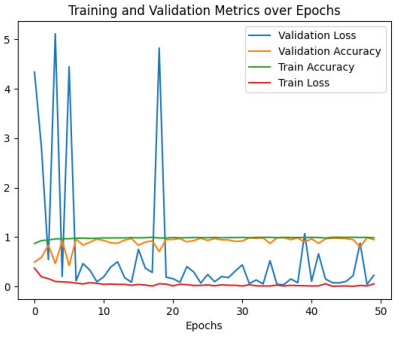

(b) GANs + DenseNet-121

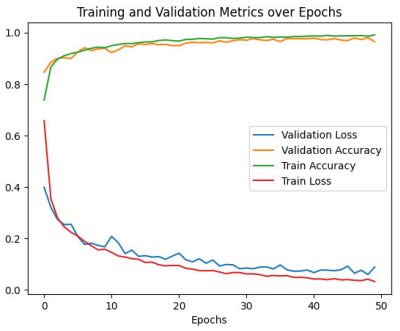

(c) GANs + MobileNet

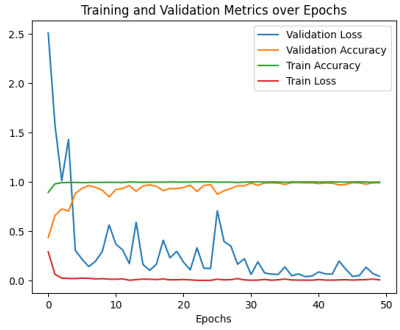

(d) GANs + MobileNet-v2

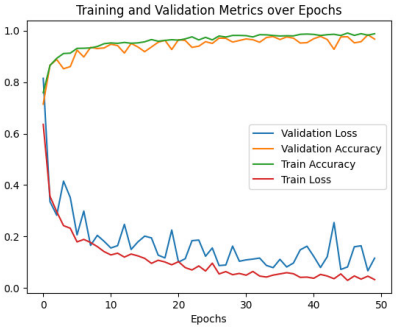

(e) GANs + VGG-19

(f) GANs + AlexNet

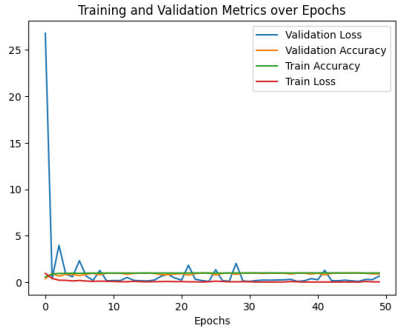

(g) GANs + Xception

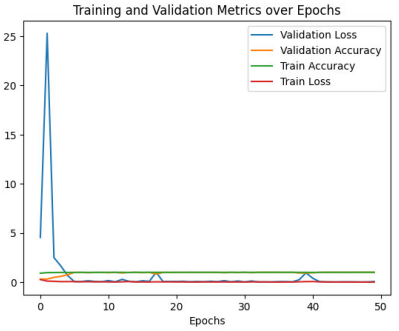

(h) GANs + ResNet-101

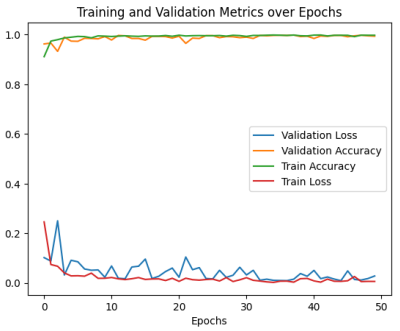

(i) GANs + Inception-v3

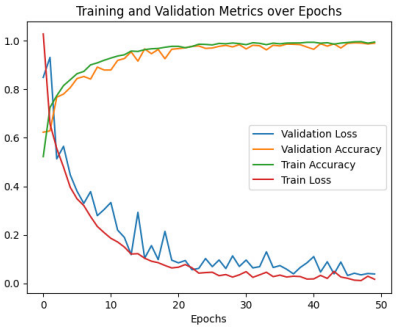

(j) Proposed TumorGANet (GANs + VGG-16)

FIGURE 7. GANs is used combined with different transfer learning model, where the training and validation model performance is shown for each model.

This operation is applied individually to each element of the output produced by every neuron. During the training phase of the TumorGANet, we fine-tune certain parameters to optimize the outcomes. Our main focus is fine-tuning

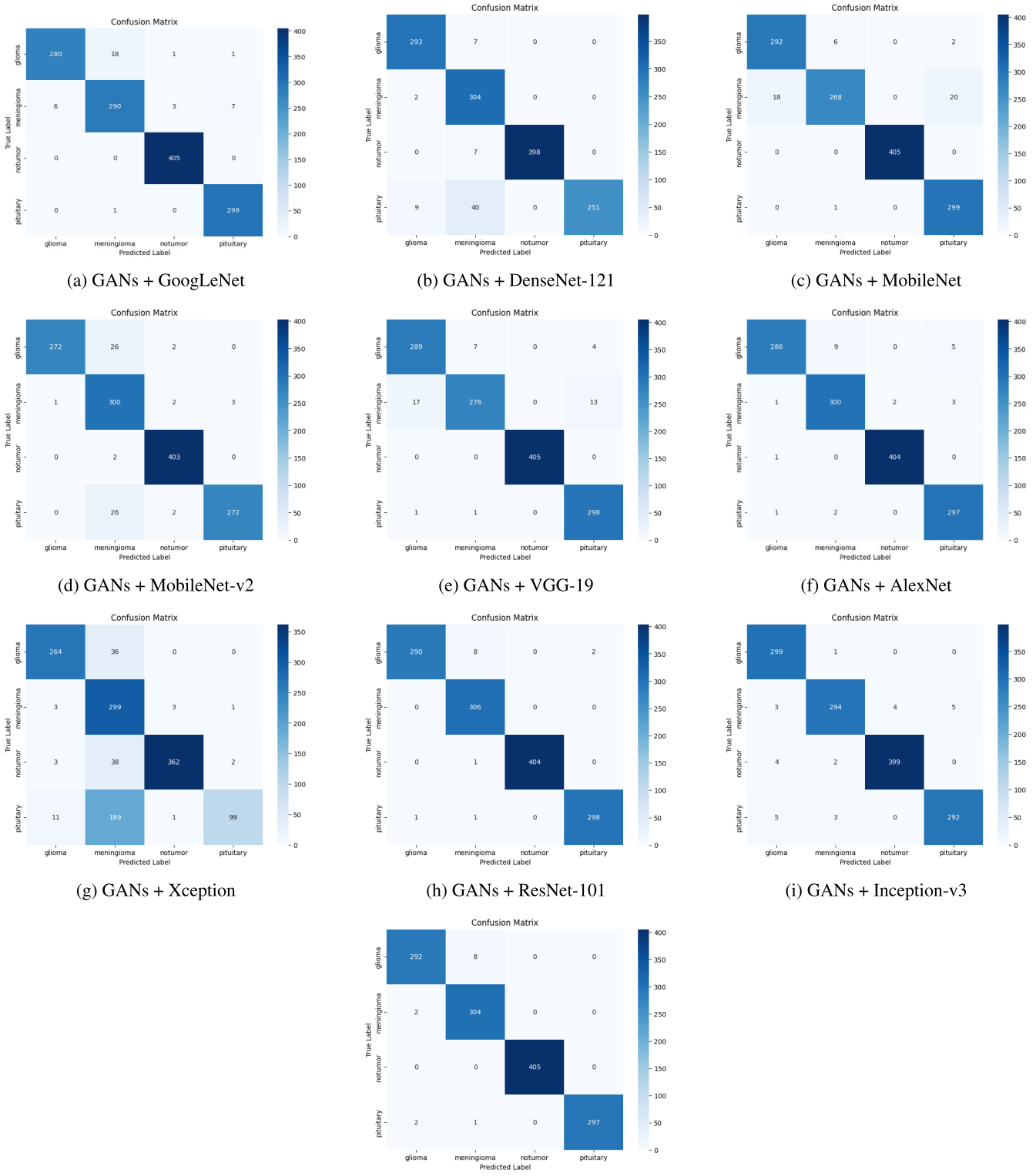

(a) GANs + GoogLeNet

(b) GANs + DenseNet-121

(c) GANs + MobileNet

(d) GANs + MobileNet-v2

(e) GANs + VGG-19

(f) GANs + AlexNet

(g) GANs + Xception

(h) GANs + ResNet-101

(i) GANs + Inception-v3

(j) Proposed TumorGANet (GANs + VGG-16)

FIGURE 8. **GANs is used combined with different transfer learning model, where confusion matrix is shown for each model.**

hyperparameters, including the number of epochs, optimizer, and learning rates. To classify among four classes, we utilize the ReLU activation function and Adam optimizer. The parameter settings are presented in Table 3.

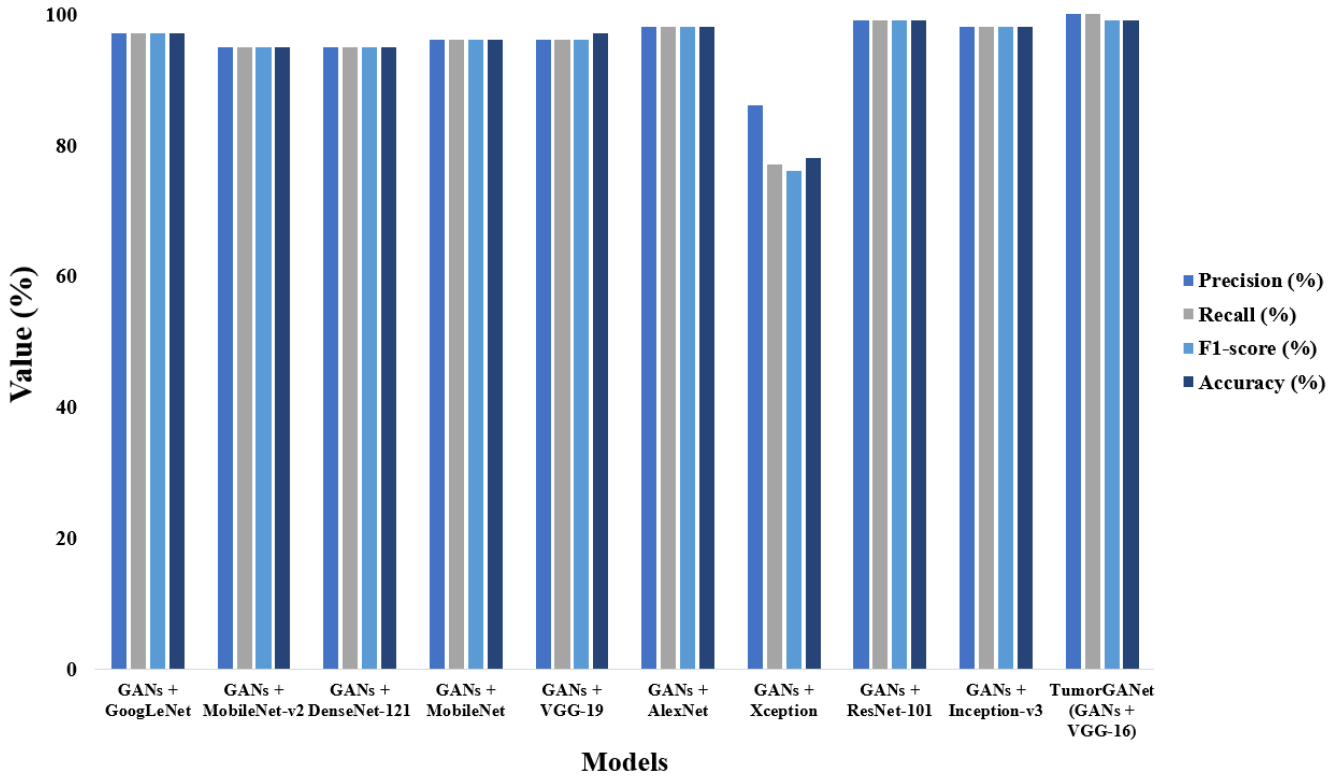

FIGURE 9. Comparison of model performance of all applied model by precision, recall, F1-Score, and accuracy.

TABLE 3. Hyperparameters of the hybrid model.

Parameters	Value
Optimizer	Adam
Dropout rate	0.5
Learning rate	0.0001
Total batch size	1024
Activation function	ReLU
Epochs	50

TABLE 4. Details about the mechanism used to carry out our approach.

Name	Experiment parameters
System type	Windows 10, 64-bit
Processor	Intel(R) Core(TM) i5-8265U CPU
SSD	512GB
RAM	16GB
Development tool	Anaconda3, and Google Colab
Hard Disk Drive	1TB

E. EXPERIMENTAL SETUP

The experiments were conducted on a computer system that had the specifications listed in Table 4.

F. PERFORMANCE EVALUATION METRICS

To evaluate the effectiveness of TumorGANet in classifying brain tumors from MRI images, many Evaluation Metrics are employed, each focusing on a certain component of its performance.

Precision, recall, F1-score, and accuracy are commonly used measures to evaluate the efficacy of image categorization models. These metrics provide a quantitative assessment of the model's capacity to accurately categorize images. The conventional mathematical methodology is utilized to evaluate these metrics, which are defined as follows: true positive (TP), false positive (FP), true negative (TN), and false negative (FN) [57].

- **Accuracy:** The *Accuracy* is a quantitative assessment of the overall effectiveness of the model. Accuracy is the degree of concordance between the model's predictions and the actual outcomes. The calculation is performed using the formula:

$$Accuracy = \frac{TP + TN}{TP + FP + TN + FN}, \tag{13}$$

- **Precision:**This metric assesses the model's ability to minimize false positives, indicating its reliability in accurately confirming tumor instances. It is characterized by a specific definition:

$$Precision = \frac{TP}{TP + FP}, \tag{14}$$

- **Recall:** Recall evaluates the model's capacity to correctly detect all instances of tumors and is defined as:

$$Recall = \frac{TP}{TP + FN}, \tag{15}$$

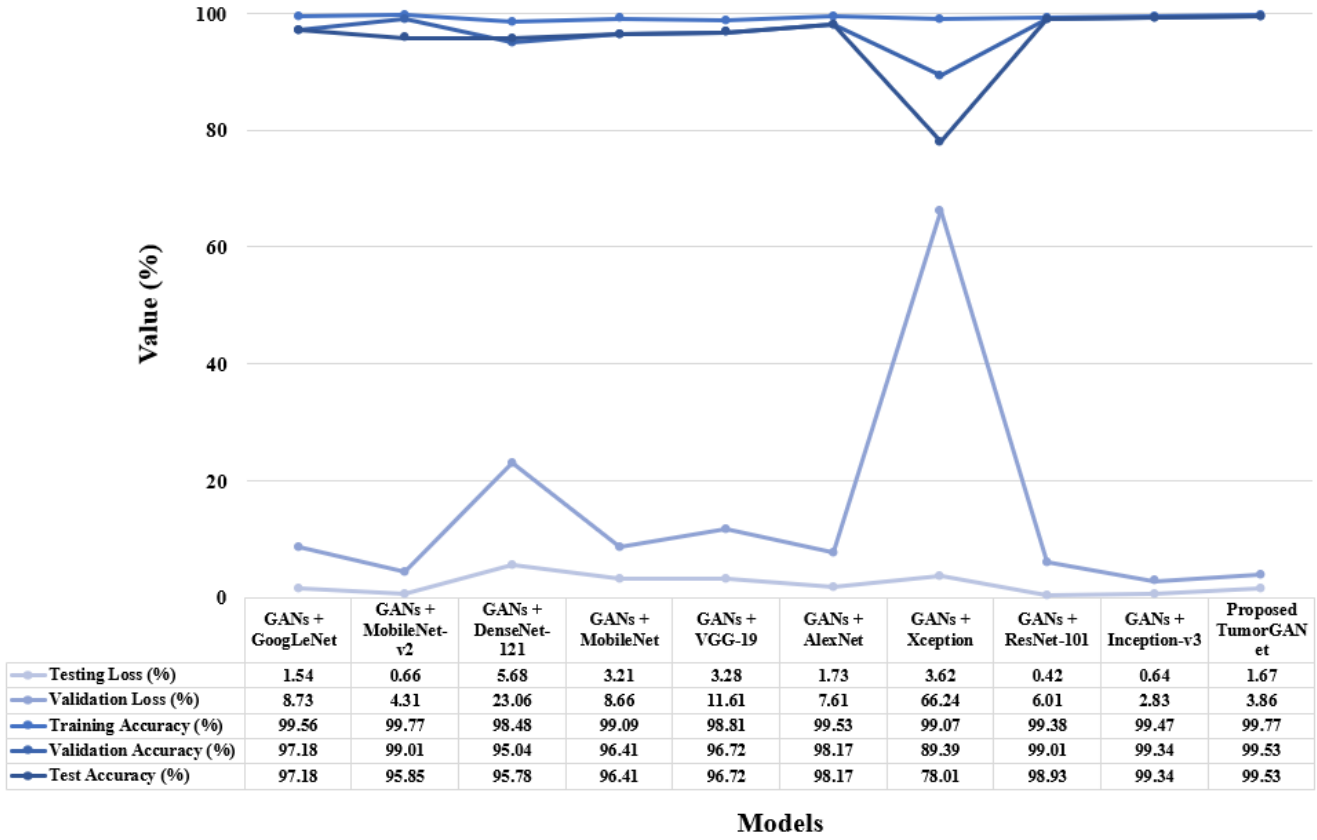

	GANs + GoogLeNet	GANs + MobileNet-v2	GANs + DenseNet-121	GANs + MobileNet	GANs + VGG-19	GANs + AlexNet	GANs + Xception	GANs + ResNet-101	GANs + Inception-v3	Proposed TumorGANet
Testing Loss (%)	1.54	0.66	5.68	3.21	3.28	1.73	3.62	0.42	0.64	1.67
Validation Loss (%)	8.73	4.31	23.06	8.66	11.61	7.61	66.24	6.01	2.83	3.86
Training Accuracy (%)	99.56	99.77	98.48	99.09	98.81	99.53	99.07	99.38	99.47	99.77
Validation Accuracy (%)	97.18	99.01	95.04	96.41	96.72	98.17	89.39	99.01	99.34	99.53
Test Accuracy (%)	97.18	95.85	95.78	96.41	96.72	98.17	78.01	98.93	99.34	99.53

FIGURE 10. Visualization for comparing all model performance by the testing loss, validation loss, training accuracy, validation accuracy, and test accuracy.

TABLE 5. All applied model's Hamming loss (*HL*), Matthews correlation coefficient (*MCC*), Jaccard score (*JS*), and Cohen's kappa values (*CK*).

Model	HL (%)	MCC (%)	JS (%)	CK (%)
GANs + GoogLeNet	2.44	94.10	90.10	93.20
GANs + MobileNet-v2	2.44	94.10	90.20	93.10
GANs + DenseNet-121	2.47	94.10	90.10	93.10
GANs + MobileNet	7.90	95.00	93.00	95.20
GANs + VGG-19	1.60	96.00	93.10	96.00
GANs + AlexNet	0.90	97.55	96.20	97.50
GANs + Xception	10.90	0.738	64.30	70.70
GANs + ResNet-101	0.50	99.10	97.90	98.70
GANs + Inception-v3	1.02	97.20	95.80	97.20
Proposed TumorGANet (GANs + VGG-16)	**00.20**	**99.50**	**98.50**	**99.50**

- **F1 Score:** The F1-Score achieves a compromise between the trade-offs of precision and recall. The harmonic mean of these two measures is calculated as follows:

$$F1score = 2 \times \frac{\text{Precision} \times \text{Recall}}{\text{Precision} + \text{Recall}}, \tag{16}$$

The F1-Score is particularly useful for imbalanced classes when both false positives and negatives are significant [43].

- **Hamming Loss (*HL*):** *HL* quantifies the mean number of erroneous class predictions made by a classifier.

$$HL = \frac{1}{n} \sum_{i=1}^{n} \mathbb{I}[y_i \neq \widehat{y_i}], \tag{17}$$

We have a dataset with $n$samples, where y_i represents the true labels for the i^{th} sample and $\widehat{y_i}$ represents the projected labels for the same i^{th} sample.

- **Jaccard Score (*JS*):** The *JS* quantifies the degree of similarity between the anticipated class labels and the

TABLE 6. Classwise model performance of all applied model by precision, recall, and F1-score values.

Model	Tumor Types	Precision (%)	Recall (%)	F1-score (%)
GANs + GoogLeNet	Glioma	98	93	96
	Meningioma	94	95	94
	No tumor	99	100	100
	Pituitary	97	100	99
GANs + MobileNet-v2	Glioma	100	91	95
	Meningioma	85	98	91
	No tumor	99	100	99
	Pituitary	99	91	95
GANs + DenseNet-121	Glioma	96	98	97
	Meningioma	85	99	92
	No tumor	100	98	99
	Pituitary	100	84	91
GANs + MobileNet	Glioma	94	97	96
	Meningioma	97	88	92
	No tumor	100	100	100
	Pituitary	93	100	96
GANs + VGG-19	Glioma	94	96	95
	Meningioma	97	90	94
	No tumor	100	100	100
	Pituitary	95	99	97
GANs + AlexNet	Glioma	99	95	97
	Meningioma	96	98	97
	No tumor	100	100	100
	Pituitary	97	99	98
GANs + Xception	Glioma	94	88	91
	Meningioma	53	98	69
	No tumor	99	89	94
	Pituitary	97	33	49
GANs + ResNet-101	Glioma	100	97	98
	Meningioma	97	100	98
	No tumor	100	100	100
	Pituitary	99	99	99
GANs + Inception-v3	Glioma	96	100	98
	Meningioma	98	96	97
	No tumor	99	99	99
	Pituitary	98	97	98
Proposed TumorGANet (GANs + VGG-16)	**Glioma**	**99**	**97**	**98**
	Meningioma	**97**	**99**	**98**
	No tumor	**100**	**100**	**100**
	Pituitary	**100**	**99**	**99**

actual class labels. The term refers to the ratio of the common elements between the expected and actual class labels, divided by the combined elements of both sets.

$$JK = \frac{|X \bigcap Y|}{|X \bigcup Y|}, \tag{18}$$

- **Matthews Correlation Coefficient (*MCC*):** *MCC* evaluates a classifier's count of TP, FP, TN, and FN predictions.

$$MCC = \frac{TP \times TN - FP \times FN}{\sqrt{(TP + FP)(TP + FN)(TN + FP)(TN + FN)}}, \tag{19}$$

- **Cohen's Kappa (*CK*):** *CK* calculates the model's predictions and real labels' agreement, allowing for random agreement. Uneven dataset classes can increase accuracy. *CK* accounts for random agreement for a more accurate image. A high *CK* value indicates great model agreement with real labels. *CK* effectively assesses categorization model reliability. This is crucial in medical diagnostics, where FP and FN have serious effects. This is its mathematical form:

$$CK = \frac{P_o - P_e}{1 - P_e}, \tag{20}$$

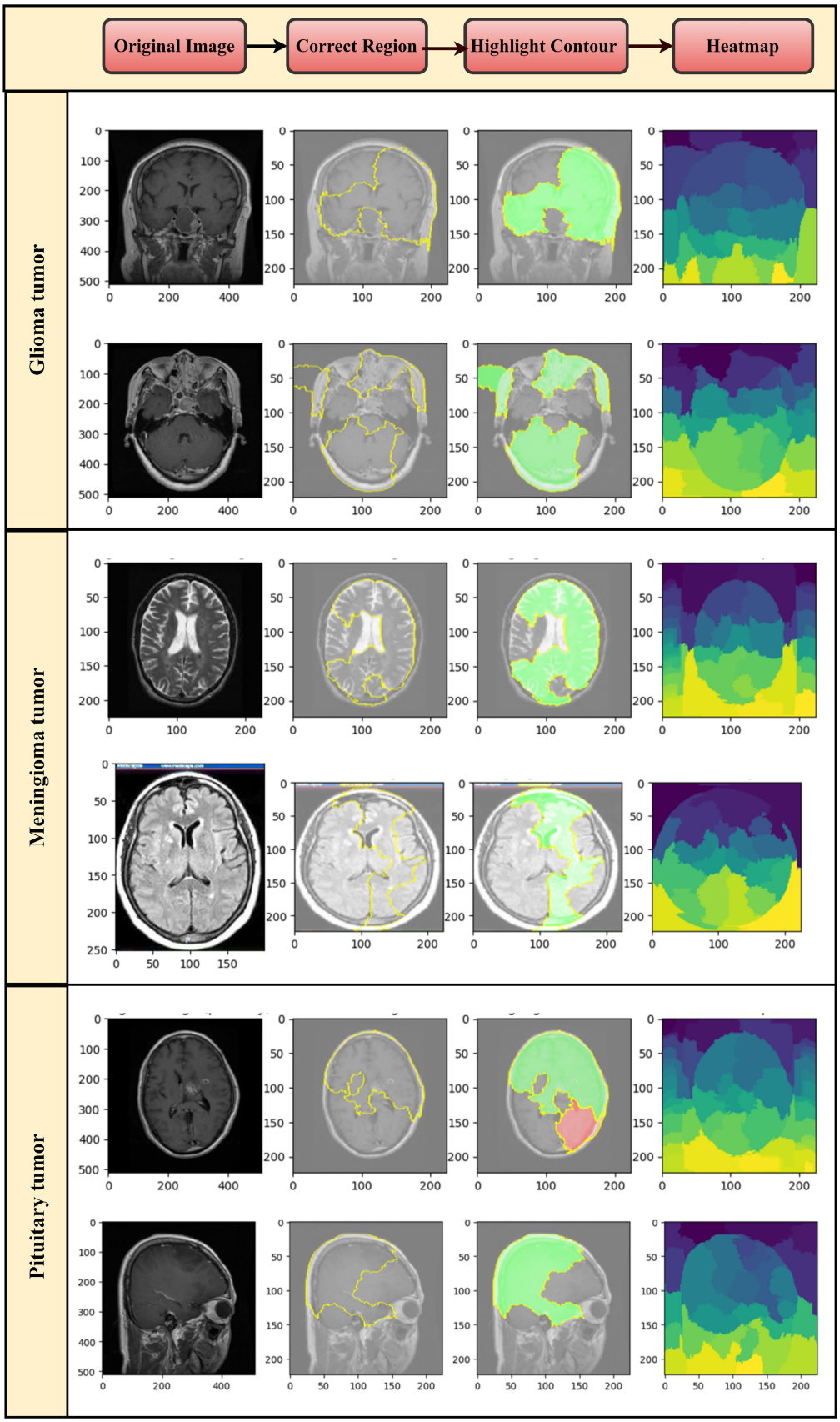

FIGURE 11. Feature explainability analysis by using LIME model.

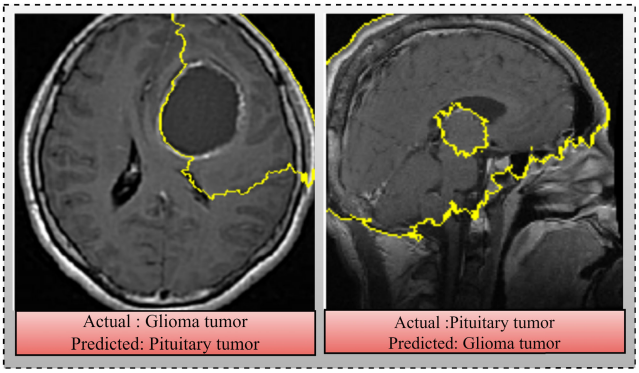

FIGURE 12. LIME based misclassification result analysis.

According to this equation, the observed agreement p_o represents the actual proportion of agreement between raters, whereas the expected agreement p_e represents the possibility of agreement by chance. The number *CK* indicates the strength of the true agreement compared to chance. A score of *1* indicates perfect agreement,*0* indicates random agreement and a negative number indicates systematic disagreement.

G. FEATURE EXPLAIN-ABILITY LOCAL INTERPRETABLE MODEL-AGNOSTIC EXPLANATIONS (LIME)

LIME is a powerful method designed to enhance the understandability of complex machine learning models at a particular level. The objective is to improve the clarity and understanding of predictions by adding the concept of local explanations. The focus is on the interpretability of individual data instances rather than the entire model. The technique operates by generating altered samples around the particular occurrence of interest, inducing random variations to the feature values. LIME is a method that accurately approximates the complex decision boundary of a model in the nearby area of a given instance without being limited to any single model. This is accomplished by implementing a locally interpretable model, typically a linear model. LIME employs kernelized weights to ensure that the perturbed samples exert a substantial influence on the local model. These weights prioritize samples that are in closer proximity to the original instance. The feature significance is assessed by examining the coefficients of this particular model, which quantifies the influence of each feature on the decision-making process. The most influential qualities, determined by their highest relevance scores, offer a localized explanation that indicates the variables with the greatest impact on the specific prognosis. LIME is useful across various industries, particularly in sensitive sectors such as healthcare or finance, where it is crucial to understand the underlying reasoning behind specific predictions [51]. LIME is essential for instilling confidence and facilitating the deployment of machine learning models in practical scenarios by providing comprehensible insights into the model's decision-making process for individual cases. The equation for LIME is as follows:

$$L(x, f, \Pi) = \sum_{i=1}^{d} \Pi_i(x) f_i(x) + C \left|\Pi\right|_1, \tag{21}$$

where, x is the instance, f is the approximation model, Π is the feature importance weights, d is the feature count, and C is a regularization parameter. The equation includes a weighted sum of features and a regularisation factor that promotes sparsity in feature weights. The optimization challenge involves determining weights Π that minimize the difference between black-box model predictions and approximation model forecasts, for instance x.

VI. OUTCOME

We predicted glioma, pituitary, meningioma, and no tumor using ten transfer learning methods. Classifier performance was measured using numerous criteria. GANs with VGG-16 performed best once the best model was found. We conducted an ablation study to determine how specific components affect ML system performance. To achieve human confidence in AI systems, LIME was used to find the best model. User-friendly models are essential. AI interpretability reveals these systems' inner workings and helps identify data leaks, model bias, robustness, and causation. The GANs + ResNet-101 model demonstrates the second-highest performance among the models. Additionally, the model achieves an average precision, recall, F1-Score, and accuracy of 99% each. In addition, the GAN s + Xception model demonstrates unsatisfactory outcomes compared to other models. The precision, recall, F1-Score, and accuracy values are all average, with percentages of 86%, 77%, 76%, and 78% respectively. The training vs validation curves for different models are shown in Figure 7 and the confusion matrices for different models are shown in Figure 8. The bar chart in Figure 9 presents the average values of classification precision, recall, F1-score, and accuracy for all models. Figure 10, displays a line chart illustrating the performance metrics of Testing Loss, Validation Loss, Training Accuracy, Validation Accuracy, and Test Accuracy. In addition, we computed the values of HL, MCC, JS, and CK for various models as shown in Table 5. The table demonstrates that our Proposed TumorGANet model, which combines GANs and VGG-19, achieves the lowest HL value while attaining the maximum MCC, JS, and CK values. Specifically, the values are 0.2% for HL, 99.50% for MCC, 98.50% for JS, and 99.50% for CK. The HL number indicates that this model has an error rate of 0.2% in its predictions. The MCC of 98.50% signifies a robust concordance between the anticipated and the factual classifications.

The average classification precision, recall, F1-Score, and accuracy for all of the models studied are displayed in Table 6 for four classes. The results demonstrate that our Proposed TumorGANet, which combines GANs with VGG-16, outperforms all other models in terms of precision, recall, F1-Score, and accuracy. Specifically, the achieved

TABLE 7. Ablation study of TumorGANet model.

Optimizer	Learning Rate	Epoch	Precision (%)	Recall (%)	F1-score (%)	Accuracy (%)	HL (%)	MCC (%)	JS (%)	CK (%)
Adam	0.001	50	100	99.00	98.00	95.00	4.70	93.70	91.00	93.60
	0.0001		99.00	100	99.00	98.00	2.20	96.00	95.00	96.00
	0.00001		**100**	**100**	**100**	**99.00**	**0.60**	**99.10**	**98.70**	**99.10**
SGD	0.001	50	100	100	100	99.00	00.40	99.30	99.00	99.30
	0.0001		100	100	100	99.00	1.30	0.981	97.30	98.10
	0.00001		94.00	100	94.00	88.00	11.70	94.30	79.40	84.20
Adagrad	0.001	50	99.00	100	99.00	98.00	1.70	97.60	96.50	97.60
	0.0001		97.00	100	96.00	88.00	11.80	84.40	78.90	84.00
	0.00001		81.00	93.00	96.00	73.00	27.00	64.40	57.10	63.50
Nadam	0.001	50	100	100	99.00	98.00	1.60	95.50	97.40	97.40
	0.0001		100	100	99.00	98.00	1.80	97.50	96.40	97.50
	0.00001		100	100	100	99.00	01.00	98.50	97.90	98.50
RMSprop	0.001	50	100	99.00	94.00	92.00	7.90	98.50	85.60	85.30
	0.0001		100	99.00	94.00	92.00	7.70	90.90	85.40	89.60
	0.00001		100	100	100	99.00	0.80	98.80	98.30	98.80

TABLE 8. Comparison of TumorGANet model with the one previously used to categorize brain tumors.

Reference	Year	Model Used	Accuracy (%)	Calculated HL	Ablation	Class-wise Classification	Feature Explainability
Tahia et al., [34]	2021	CNN	92	No	No	Yes	No
Lamrani et al., [36]	2022	CNN	96	No	No	No	No
Nayak et al., [39]	2022	Deep autoencoder approach	97	No	No	No	No
Kokkalla et al., [40]	2021	Deep inception residual network	97.69	No	No	No	No
Kesav et al., [41]	2022	RCNN-based model	98.21	No	No	No	No
Krishnasamy, N. et al., [44]	2023	FCNs + ResNet	93.90	No	No	No	Yes
Ullah N et al., [46]	2022	Inceptionresnetv2	98.91	No	No	No	No
Gaikwad, S. et al., [49]	2023	EfficientNetV2B1	97.40	No	No	No	No
Ullah N et al., [50]	2024	DeepEBTDNet	98.96	No	No	No	Yes
Haque, R., et al., [51]	2024	NeuroNet19	99.30	No	Yes	No	Yes
Ullah N et al., [52]	2022	TumorResNet	99.33	No	Yes	No	No
Proposed	**2024**	**TumorGANet**	**99.53**	**Yes**	**Yes**	**Yes**	**Yes (LIME)**

values for these metrics are 100%, 100%, 99%, and 99%, respectively. An F1-Score of 99% indicates a favorable equilibrium between precision and recall. Furthermore, the model exhibits a 99% accuracy rate in accurately predicting classes.

VII. ABLATION STUDY

Ablation study is a systematic way to assess and isolate the contributions of model components, features, and aspects in machine learning. This procedure reveals how these factors affect model performance. This experimental method involves deliberately removing or altering model architecture, training procedure, or input properties to assess performance measurements. The key goal is to understand the model's decision-making process and determine which elements influence forecasts [44]. Ablation studies can improve machine learning model comprehensibility by revealing feature importance, model robustness, and component sensitivity. In this research, we utilized five different optimizes and three distinct learning rates, with the epoch fixed. Table 7 presents the results of the ablation study conducted on the TumorGANet model. We maintain a constant Epoch while altering the Optimizer and Learning Rate. Significant values are shown in bold.

VIII. FEATURES EXPLAINABILITY ANALYSIS

Figure 11, shows LIME-generated images. The display only shows super-pixels in the correct region, complete with highlighted contours and background. The image showed green super-pixels in the correlation portion, indicating a higher likelihood of belonging to a specific class. Meanwhile, red super-pixels indicate a drop in probability. LIME generates heat maps by overlaying a transparent mask on the original image, with the mask's transparency indicating the significance of each feature. The more transparent sections represent the most significant elements. LIME generates heat maps by selecting a local region around the prediction and training a basic linear model. Model misclassified photos in Figure 12 exhibit continuous patterns or trends in attributes that led to erroneous predictions. To prevent future errors, the model should be updated and training data quality improved.

IX. COMPARISON WITH STATE-OF-THE-ART METHODS

In this study, we utilized a Brain MRI dataset consisting of 7023 pictures, which is significantly larger than the datasets used in earlier research. Class-wise analyses were performed to evaluate precision, recall, and F1-score for each type of tumor, namely glioma, meningioma, and pituitary cancers, as well as for the absence of tumors in TumorGANet. Prior techniques employing transfer learning, as outlined in Haque R., et al., [51], did not compare the performance class-wise on the same dataset. An ablation was conducted on the TumorGANet model, utilizing five distinct optimizers: Adam, SGD, Adagrad, Nadam, and RMSprop, each with three varying learning rates. This ablation analysis

showcases the robustness of TumorGANet. The TumorGANet model and the previously used method for brain tumor classification are compared in Table 8. TumorGANet demonstrates a remarkable accuracy of 99.53%. We have computed the numerical value of HL. None of the earlier models mentioned in Table 8 computed the HL. In addition, we utilize LIME to do analysis, identify important features, and present both correctly identified and misclassified instances.

X. DISCUSSION

This study presents a TumorGANet which is a DL framework that outperformed other methods for BT classification from MRI, with training and testing accuracy levels of 99.77% and 99.53%, respectively. The TumorGANet utilized ResNet-50 to extract features from the dataset and then employed GANs for data augmentation to boost the model's capabilities. Finally, VGG-16 was used to categorize BT. This architecture for TumorGANet uses the following parameters: Optimizer Adam, 0.5 dropout rate, 0.0001 learning rate, 1024 total batches, ReLU activation function, and 50 epochs. TumorGANet used GANs-based augmentation approaches over other augmentation methods because GANs generate synthetic data that closely resembles the original dataset, capturing its underlying distribution more accurately compared to simple transformations like rotation or flipping. It can produce a wide variety of realistic data samples, introducing diverse variations and complexities that help improve the model's robustness and generalization. GANs can also generate data tailored to specific features, allowing for more effective augmentation based on the desired attributes. With this, TumorGANet can more accurately detect BT than previously developed models.

The new TumorGANet model helps classify BT better, but it might not work well with all types of data. Real-world differences in how images are taken and tumor types could make it harder for the model to work everywhere. Although GANs can enhance data augmentation, there is a potential for introducing synthetic features or artifacts that may not faithfully depict actual tumors. Thorough validation and rigorous quality control of augmented data are crucial. Training and deploying DL models, particularly those utilizing architectures such as ResNet50 and GANs, can incur significant computational costs. This may restrict the availability of the model, particularly in contexts with limited resources. Also, it needs a lot of special knowledge, which might be tough for some people to use.

XI. CONCLUSION

TumorGANet presents an innovative approach for categorizing BT by employing state-of-the-art techniques in MRI-based analysis. This research combines innovative strategies, utilizing the capabilities of deep learning and transfer learning paradigms, to address the limitations associated with traditional approaches. This study enhances the strength and diversity of the dataset by using pre-processing techniques and utilizing data augmentation with GANs. To determine which features are important for prediction, we also employ LIME. In addition to showcasing the model's transparency using LIME, our suggested model, TumorGANet, showcases the model's advanced proficiency in classification tasks. A low rate of tumor identification mistakes is achieved by the proposed model, TumorGANet, due to its high degree of accuracy. To ensure that patients receive accurate and timely treatment, the model examines the findings of MRI scans to enhance categorization and decrease the number of false negatives. When it comes to analyzing MRI scans, TumorGANet achieves the highest accuracy at 99.53%, with precision and recall at 100%, F1 scores at 99%, and Hamming Loss at 0.2%. To publish our model globally and enable its continual refinement through the development of an expert BT classification system. This application can enhance the accuracy of BT diagnosis for medical specialists and clinicians. We aim to integrate federated learning and digital twins into this expert system in the future.

XII. FUTURE WORK

Future research will focus on integrating federated learning into TumorGANet to enhance data privacy and security, enabling the model to learn from diverse datasets without compromising patient confidentiality. Incorporating digital twin technology is another priority, providing dynamic, real-time simulations of patient conditions for personalized treatment planning. Expanding the dataset to include more diverse MRI scans from various sources will further validate and enhance the model's robustness. Additionally, real-time implementation and clinical trials are planned to assess TumorGANet's performance in practical settings, ensuring its efficacy in improving brain tumor diagnosis and treatment.

DATA AVAILABILITY STATEMENT

The used dataset of this study "Brain Tumor MRI Dataset" is publicly available at https://www.kaggle.com/datasets/masoudnickparvar/brain-tumor-mri-dataset with the DOI [https://doi.org/10.34740/kaggle/dsv/2645886]. The code associated with this research is found at the link [https://github.com/Hirak46/TumorGANet], with the special request of the corresponding authors.

ACKNOWLEDGMENT

The authors express their thanks to the Researchers Supporting Project number (RSP2024R206), King Saud University, Riyadh, Saudi Arabia. Also we extend our sincere gratitude to the Ministry of Science and Technology, Government of Bangladesh for their support, enabling the research conducted under the NST fellowship program.

AUTHOR CONTRIBUTION

Anindya Nag: Conceptualization, Methodology, Software, Visualization, Writing—Original draft preparation, and editing. **Hirak Mondal:** Methodology, Formal Analysis,

Software, and Visualization. **Md Mehedi Hassan:** Conceptualization, Methodology, Formal Analysis, Project administration, and Writing—Original draft preparation. **Taher Al-Shehari, Mohammed Kadrie, and Muna Al-Razgan:** Funding, Writing—reviewing and editing. **Sujit Biswas:** Writing—reviewing and editing. **Anupam Kumar Bairagi:** Supervising, Writing-reviewing, and editing.

REFERENCES

[1] H. Mohsen, E.-S.-A. El-Dahshan, E.-S.-M. El-Horbaty, and A.-B.-M. Salem, "Classification using deep learning neural networks for brain tumors," *Future Comput. Informat. J.*, vol. 3, no. 1, pp. 68–71, Jun. 2018.

[2] A. Isin, C. Direkoglu, and M. Sah, "Review of MRI-based brain tumor image segmentation using deep learning methods," *Proc. Comput. Sci.*, vol. 102, pp. 317–324, Jan. 2016.

[3] (Jun. 2023). *Source K: Brain Tumour Statistics*. [Online]. Available: https://assets.thebraintumourcharity.org/live/uploads/2023/06/Source-K_-Brain-Tumour-Statistics-June-2023-Final-Version.pdf

[4] American Cancer Society. *Cancer Facts & Figures 2023*. [Online]. Available: https://www.cancer.org/research/cancer-facts-statistics/all-cancer-facts-figures/2023-cancer-facts-figures.html

[5] H. E. M. Abdalla and M. Y. Esmail, "Brain tumor detection by using artificial neural network," in *Proc. Int. Conf. Comput., Control, Electr., Electron. Eng. (ICCCEEE)*, Aug. 2018, pp. 1–6.

[6] S. Hussain, S. M. Anwar, and M. Majid, "Segmentation of glioma tumors in brain using deep convolutional neural network," *Neurocomputing*, vol. 282, pp. 248–261, Mar. 2018.

[7] J. Liu, H. Liu, Z. Tang, W. Gui, T. Ma, S. Gong, Q. Gao, Y. Xie, and J. P. Niyoyita, "IOUC-3DSFCNN: Segmentation of brain tumors via IOU constraint 3D symmetric full convolution network with multimodal auto-context," *Sci. Rep.*, vol. 10, no. 1, p. 6256, Apr. 2020.

[8] X. Zhao, Y. Wu, G. Song, Z. Li, Y. Zhang, and Y. Fan, "A deep learning model integrating FCNNs and CRFs for brain tumor segmentation," *Med. Image Anal.*, vol. 43, pp. 98–111, Jan. 2018.

[9] J. Amin, M. Sharif, M. Yasmin, and S. L. Fernandes, "Big data analysis for brain tumor detection: Deep convolutional neural networks," *Future Gener. Comput. Syst.*, vol. 87, pp. 290–297, Oct. 2018.

[10] D. Nie, H. Zhang, E. Adeli, L. Liu, and D. Shen, "3D deep learning for multi-modal imaging-guided survival time prediction of brain tumor patients," in *Proc. 19th Int. Conf.* Athens, Greece: Springer, Oct. 2016, pp. 212–220.

[11] S. Pereira, A. Pinto, V. Alves, and C. A. Silva, "Brain tumor segmentation using convolutional neural networks in MRI images," *IEEE Trans. Med. Imag.*, vol. 35, no. 5, pp. 1240–1251, May 2016.

[12] S. Lu, Z. Lu, and Y.-D. Zhang, "Pathological brain detection based on AlexNet and transfer learning," *J. Comput. Sci.*, vol. 30, pp. 41–47, Jan. 2019.

[13] B. Chen, L. Zhang, H. Chen, K. Liang, and X. Chen, "A novel extended Kalman filter with support vector machine based method for the automatic diagnosis and segmentation of brain tumors," *Comput. Methods Programs Biomed.*, vol. 200, Mar. 2021, Art. no. 105797.

[14] G. T. Woldeyohannes and S. P. Pati, "Brain MRI classification for detection of brain tumors using hybrid feature extraction and SVM," in *Proc. Intell. Cloud Comput. (ICICC)*, 2021, pp. 571–579.

[15] S. Saeed, A. Abdullah, N. Z. Jhanjhi, M. Naqvi, and A. Nayyar, "New techniques for efficiently k-NN algorithm for brain tumor detection," *Multimedia Tools Appl.*, vol. 81, no. 13, pp. 18595–18616, May 2022.

[16] T. Rahman and M. S. Islam, "MRI brain tumor detection and classification using parallel deep convolutional neural networks," *Meas., Sensors*, vol. 26, Apr. 2023, Art. no. 100694.

[17] M. O. Khairandish, M. Sharma, V. Jain, J. M. Chatterjee, and N. Z. Jhanjhi, "A hybrid CNN-SVM threshold segmentation approach for tumor detection and classification of MRI brain images," *IRBM*, vol. 43, no. 4, pp. 290–299, Aug. 2022.

[18] M. Sunil Babu and V. Vijayalakshmi, "An effective approach for sub-acute ischemic stroke lesion segmentation by adopting meta-heuristics feature selection technique along with hybrid naive Bayes and sample-weighted random forest classification," *Sens. Imag.*, vol. 20, no. 1, pp. 1–24, Dec. 2019.

[19] S. Asif, W. Yi, Q. U. Ain, J. Hou, T. Yi, and J. Si, "Improving effectiveness of different deep transfer learning-based models for detecting brain tumors from MR images," *IEEE Access*, vol. 10, pp. 34716–34730, 2022.

[20] Y. L. Wang, Z. J. Zhao, S. Y. Hu, and F. L. Chang, "CLCU-net: Cross-level connected U-shaped network with selective feature aggregation attention module for brain tumor segmentation," *Comput. Methods Programs Biomed.*, vol. 207, Aug. 2021, Art. no. 106154.

[21] J. Sun, Y. Peng, Y. Guo, and D. Li, "Segmentation of the multimodal brain tumor image used the multi-pathway architecture method based on 3D FCN," *Neurocomputing*, vol. 423, pp. 34–45, Jan. 2021.

[22] L. H. Shehab, O. M. Fahmy, S. M. Gasser, and M. S. El-Mahallawy, "An efficient brain tumor image segmentation based on deep residual networks (ResNets)," *J. King Saud Univ.-Eng. Sci.*, vol. 33, no. 6, pp. 404–412, Sep. 2021.

[23] M. U. Rehman, S. Cho, J. Kim, and K. T. Chong, "BrainSeg-net: Brain tumor MR image segmentation via enhanced encoder–decoder network," *Diagnostics*, vol. 11, no. 2, p. 169, Jan. 2021.

[24] Z. A. Al-Saffar and T. Yildirim, "A novel approach to improving brain image classification using mutual information-accelerated singular value decomposition," *IEEE Access*, vol. 8, pp. 52575–52587, 2020.

[25] A. Deshpande, V. V. Estrela, and P. Patavardhan, "The DCT-CNN-ResNet50 architecture to classify brain tumors with super-resolution, convolutional neural network, and the ResNet50," *Neurosci. Informat.*, vol. 1, no. 4, Dec. 2021, Art. no. 100013.

[26] V. Pooja, M. K. Kumar, and K. Kamalesh, "Comparative analysis of segmentation techniques on MRI brain tumor images," *Mater. Today, Proc.*, vol. 47, pp. 109–114, Jan. 2021.

[27] H. A. Shah, F. Saeed, S. Yun, J.-H. Park, A. Paul, and J.-M. Kang, "A robust approach for brain tumor detection in magnetic resonance images using finetuned EfficientNet," *IEEE Access*, vol. 10, pp. 65426–65438, 2022.

[28] M. I. Mahmud, M. Mamun, and A. Abdelgawad, "A deep analysis of brain tumor detection from MR images using deep learning networks," *Algorithms*, vol. 16, no. 4, p. 176, Mar. 2023.

[29] B. Srikanth and S. V. Suryanarayana, "WITHDRAWN: Multi-class classification of brain tumor images using data augmentation with deep neural network," *Mater. Today, Proc.*, Mar. 2021.

[30] N. A. Samee, N. F. Mahmoud, G. Atteia, H. A. Abdallah, M. Alabdulhafith, M. S. A. M. Al-Gaashani, S. Ahmad, and M. S. A. Muthanna, "Classification framework for medical diagnosis of brain tumor with an effective hybrid transfer learning model," *Diagnostics*, vol. 12, no. 10, p. 2541, Oct. 2022.

[31] R. K. Gupta, S. Bharti, N. Kunhare, Y. Sahu, and N. Pathik, "Brain tumor detection and classification using cycle generative adversarial networks," *Interdiscipl. Sci., Comput. Life Sci.*, vol. 14, no. 2, pp. 485–502, Jun. 2022.

[32] S. Alqazzaz, X. Sun, X. Yang, and L. Nokes, "Automated brain tumor segmentation on multi-modal MR image using SegNet," *Comput. Vis. Media*, vol. 5, no. 2, pp. 209–219, Jun. 2019.

[33] C. Öksüz, O. Urhan, and M. K. Güllü, "Brain tumor classification using the fused features extracted from expanded tumor region," *Biomed. Signal Process. Control*, vol. 72, Feb. 2022, Art. no. 103356.

[34] T. Tazin, S. Sarker, P. Gupta, F. I. Ayaz, S. Islam, M. Monirujjaman Khan, S. Bourouis, S. A. Idris, and H. Alshazly, "A robust and novel approach for brain tumor classification using convolutional neural network," *Comput. Intell. Neurosci.*, vol. 2021, pp. 1–11, Dec. 2021.

[35] R. Hashemzehi, S. J. S. Mahdavi, M. Kheirabadi, and S. R. Kamel, "Detection of brain tumors from MRI images base on deep learning using hybrid model CNN and NADE," *Biocybernetics Biomed. Eng.*, vol. 40, no. 3, pp. 1225–1232, Jul. 2020.

[36] D. Lamrani, B. Cherradi, O. E. Gannour, M. A. Bouqentar, and L. Bahatti, "Brain tumor detection using MRI images and convolutional neural network," *Int. J. Adv. Comput. Sci. Appl.*, vol. 13, no. 7, pp. 452–460, 2022.

[37] S. Kadry, Y. Nam, H. T. Rauf, V. Rajinikanth, and I. A. Lawal, "Automated detection of brain abnormality using deep-learning-scheme: A study," in *Proc. 7th Int. Conf. Bio Signals, Images, Instrum. (ICBSII)*, Mar. 2021, pp. 1–5.

[38] S. A. Abdelaziz Ismael, A. Mohammed, and H. Hefny, "An enhanced deep learning approach for brain cancer MRI images classification using residual networks," *Artif. Intell. Med.*, vol. 102, Jan. 2020, Art. no. 101779.
[39] D. R. Nayak, N. Padhy, P. K. Mallick, and A. Singh, "A deep autoencoder approach for detection of brain tumor images," *Comput. Electr. Eng.*, vol. 102, Sep. 2022, Art. no. 108238.
[40] S. Kokkalla, J. Kakarla, I. B. Venkateswarlu, and M. Singh, "Three-class brain tumor classification using deep dense inception residual network," *Soft Comput.*, vol. 25, no. 13, pp. 8721–8729, Jul. 2021.
[41] N. Kesav and M. G. Jibukumar, "Efficient and low complex architecture for detection and classification of brain tumor using RCNN with two channel CNN," *J. King Saud Univ.-Comput. Inf. Sci.*, vol. 34, no. 8, pp. 6229–6242, Sep. 2022.
[42] T. M. Ali, A. Nawaz, A. Ur Rehman, R. Z. Ahmad, A. R. Javed, T. R. Gadekallu, C.-L. Chen, and C.-M. Wu, "A sequential machine learning-cum-attention mechanism for effective segmentation of brain tumor," *Frontiers Oncol.*, vol. 12, Jun. 2022, Art. no. 873268.
[43] J. Hong, Y. Huang, J. Ye, J. Wang, X. Xu, Y. Wu, Y. Li, J. Zhao, R. Li, J. Kang, and X. Lai, "3D FRN-ResNet: An automated major depressive disorder structural magnetic resonance imaging data identification framework," *Frontiers Aging Neurosci.*, vol. 14, May 2022, Art. no. 912283.
[44] S. R. Krishna, C. Ravela, S. V. Mantena, M. Sirajuddin, and G. J. S. Deol, "Deep learning-based robust hybrid approaches for brain tumor classification in magnetic resonance images," *J. Inst. Eng. (India), Ser. B*, vol. 33, no. 6, pp. 2157–2177, Sep. 2023.
[45] U. Zahid, I. Ashraf, M. A. Khan, M. Alhaisoni, K. M. Yahya, H. S. Hussein, and H. Alshazly, "BrainNet: Optimal deep learning feature fusion for brain tumor classification," *Comput. Intell. Neurosci.*, vol. 2022, pp. 1–13, Aug. 2022.
[46] N. Ullah, J. A. Khan, M. S. Khan, W. Khan, I. Hassan, M. Obayya, N. Negm, and A. S. Salama, "An effective approach to detect and identify brain tumors using transfer learning," *Appl. Sci.*, vol. 12, no. 11, p. 5645, Jun. 2022.
[47] S. Tummala, S. Kadry, S. A. C. Bukhari, and H. T. Rauf, "Classification of brain tumor from magnetic resonance imaging using vision transformers ensembling," *Current Oncol.*, vol. 29, no. 10, pp. 7498–7511, Oct. 2022.
[48] N. Cinar, A. Ozcan, and M. Kaya, "A hybrid DenseNet121-UNet model for brain tumor segmentation from MR images," *Biomed. Signal Process. Control*, vol. 76, Jul. 2022, Art. no. 103647.
[49] S. Gaikwad, S. Patel, and A. Shetty, "Brain tumor detection: An application based on machine learning," in *Proc. 2nd Int. Conf. Emerg. Technol. (INCET)*, May 2021, pp. 1–4.
[50] N. Ullah, M. Hassan, J. A. Khan, M. S. Anwar, and K. Aurangzeb, "Enhancing explainability in brain tumor detection: A novel DeepEBTD-Net model with LIME on MRI images," *Int. J. Imag. Syst. Technol.*, vol. 34, no. 1, Jan. 2024, Art. no. e23012.
[51] R. Haque, M. M. Hassan, A. K. Bairagi, and S. M. S. Islam, "NeuroNet19: An explainable deep neural network model for the classification of brain tumors using magnetic resonance imaging data," *Sci. Rep.*, vol. 14, no. 1, p. 1524, Jan. 2024.
[52] N. Ullah, M. S. Khan, J. A. Khan, A. Choi, and M. S. Anwar, "A robust end-to-end deep learning-based approach for effective and reliable BTD using MR images," *Sensors*, vol. 22, no. 19, p. 7575, Oct. 2022.
[53] A. Raza, H. Ayub, J. A. Khan, I. Ahmad, A. S. Salama, Y. I. Daradkeh, D. Javeed, A. U. Rehman, and H. Hamam, "A hybrid deep learning-based approach for brain tumor classification," *Electronics*, vol. 11, no. 7, p. 1146, Apr. 2022.
[54] M. M. Haque, S. K. Paul, R. R. Paul, N. Islam, M. A. F. M. R. Hasan, and M. E. Hamid, "Improving performance of a brain tumor detection on MRI images using DCGAN-based data augmentation and vision transformer (ViT) approach," in *GANs for Data Augmentation in Healthcare*. Cham, Switzerland: Springer, 2023, pp. 157–186.
[55] P. Datta and R. Rohilla, "Brain tumor image pixel segmentation and detection using an aggregation of GAN models with vision transformer," *Int. J. Imag. Syst. Technol.*, vol. 34, no. 1, Jan. 2024, Art. no. e22979.
[56] P. Ghosh, A. K. Mondal, S. Chatterjee, M. Masud, H. Meshref, and A. K. Bairagi, "Recognition of sunflower diseases using hybrid deep learning and its explainability with AI," *Mathematics*, vol. 11, no. 10, p. 2241, May 2023.
[57] M. M. Rana, M. M. Islam, M. A. Talukder, M. A. Uddin, S. Aryal, N. Alotaibi, S. A. Alyami, K. F. Hasan, and M. A. Moni, "A robust and clinically applicable deep learning model for early detection of Alzheimer's," *IET Image Process.*, vol. 17, no. 14, pp. 3959–3975, Dec. 2023.

ANINDYA NAG (Member, IEEE) received the B.Tech. degree from Adamas University, Kolkata, India. He is pursuing the M.Sc. degree in computer science and engineering with Khulna University, Bangladesh. He was nominated for the dean's list due to his exceptional academic performance. His research interests include wireless resource management in 6G and future generations, healthcare, the Industrial Internet of Things (IIoT), Medical Internet of Things (MIoT), natural language processing (NLP), machine learning, deep learning, artificial intelligence (AI), blockchain, cloud computing, and networking systems. He serves as a reviewer for various reputable journals and international conferences. He has written and collaborated on approximately 30 articles, which include peer-reviewed journals and conference papers published by IEEE.

HIRAK MONDAL is currently pursuing the B.Sc. degree in computer science and engineering with North Western University, Khulna, Bangladesh. His journey in the realm of technology is marked by a fervent dedication to research, with a specific focus on the intersection of healthcare, machine learning, the IoT, and deep learning. He believes in the power of collaborative innovation and his journey reflects a relentless pursuit of solutions that bridge the gap between technology and human well-being. He is motivated by the aspiration to make significant contributions to groundbreaking improvements, whether it involves using machine learning to understand healthcare intricacies or using IoT and deep learning.

MD MEHEDI HASSAN (Member, IEEE) received the B.Sc. degree in computer science and engineering from North Western University, Khulna, in 2022, where he excelled in his studies and demonstrated a strong aptitude for research and the Master of Science (M.Sc.) degree in computer science and engineering from Khulna University, Khulna, Bangladesh, in 2024. He is currently a Dedicated and Accomplished Researcher. As the Founder and the CEO of The Virtual BD IT Firm and VRD Research Laboratory, Bangladesh, he has established himself as a Highly Respected Leader in the fields of biomedical engineering, data science, and expert systems. His research interests include important human diseases, such as oncology, cancer, hepatitis, and human behavior analysis and mental health. He is highly skilled in association rule mining, predictive analysis, machine learning, and data analysis, with a particular focus on the biomedical sciences. As a young researcher, he has published 54 articles in various international top journals and conferences, which is a remarkable achievement. His work has been well-received by the research community and has significantly contributed to the advancement of knowledge in his field. Overall, he is a highly motivated and skilled researcher with a strong commitment to improving human health and well-being through cutting-edge scientific research. His accomplishments to date are impressive and his potential for future contributions to his field is very promising. Additionally, he serves as an academic editor and a reviewer for 56 prestigious journals. He has filed more than three patents out of which three are granted to his name.

TAHER AL-SHEHARI received the B.Sc. degree in computer science from King Khalid University, Saudi Arabia, in 2007, and the M.S. degree in computer science from the King Fahd University of Petroleum and Minerals (KFUPM), in 2014. From 2011 to 2014, he was a Research Assistant at the King Fahd University of Petroleum and Minerals. Since 2015, he is working as a Senior Lecturer and Researcher at King Saud University. He is the author of several papers that are published in prestige journals. His research interests include information security and privacy, insider threat detection and prevention systems, machine learning models, and data analysis. His awards and honors include an Honor Award from King Khalid University's Rector, and Best Designed Curriculum Award from CFY's Dean, KSU.

MOHAMMED KADRIE received the B.S. degree in mathematics and informatics from the Faculty of Sciences, Aleppo University, Aleppo, Syria, in 1990, the D.E.A. degree in informatics from ESSI High School, UNSA University, Nice, French, in 1998, and the Ph.D. degree in informatics from UNSA University, Nice, French, in 2002. He was a Teacher in informatics from Teacher's Colleges, King Saud University, Riyadh, SA., from 2010 to 2015. His research interest includes The Theory of Codes, Automata, and Artificial Intelligence.

MUNA AL-RAZGAN received the Ph.D. degree in information technology from George Mason University, VA, USA. She is currently an Associate Professor in software engineering with the College of Computer and Information Sciences, King Saud University, Riyadh, Saudi Arabia. Her research interests include data mining, machine learning, artificial intelligence, educational data mining, and assistive technologies.

TAHA ALFAKIH received the B.S. degree in computer science from the Computer Science Department, Hadhramout University, Yemen, and the M.Sc. and Ph.D. degrees from King Saud University (KSU). His research interests include machine learning, mobile edge computing, and the Internet of Things (IoT).

SUJIT BISWAS (Member, IEEE) received the Ph.D. degree in computer science and technology from Beijing Institute of Technology, China. He is currently a Lecturer with the Cyber Security and Fintech, Computer Science Department, City, University of London, U.K. He is also an Assistant Professor with the Faridpur Engineering College, University of Dhaka, Bangladesh. His research interests include the IoT, blockchain, sensor networks, machine learning, federated learning, and deep learning. He is a Life Member of Bangladesh Computer Society (BCS).

ANUPAM KUMAR BAIRAGI (Senior Member, IEEE) received the B.Sc. and M.Sc. degrees in computer science and engineering from Khulna University (KU), Bangladesh, and the Ph.D. degree in computer engineering from Kyung Hee University, South Korea. He is currently a Professor with the Computer Science and Engineering Discipline, KU. His research interests include wireless resource management in 5G and beyond, healthcare, the IIoT, cooperative communication, and game theory. He has authored or co-authored around 60 publications, including refereed IEEE/ACM journals, and conference papers. He has served as a technical program committee member for different international conferences.